International Journal of Mechanical Sciences 137 (2018) 24–45

Contents lists available at ScienceDirect

International Journal of Mechanical Sciences

journal homepage: www.elsevier.com/locate/ijmecsci

Modelling and simulation of a stationary high-rise elevator system to predict the dynamic interactions between its components

Rafael Sanchez Crespo*, Stefan Kaczmarczyk*, Phil Picton, Huijuan Su

Faculty of Arts, Science and Technology, The University of Northampton, Avenue Campus, St George's Avenue, NN2 6JD Northampton, United Kingdom

ARTICLE INFO

Keywords:
Rope vibration
Modelling
Numerical simulation
High-rise elevator system
Nonlinear dynamic interactions
Curve veering phenomena

ABSTRACT

In a high-rise elevator system lateral vibrations of the suspension and compensating ropes, coupled with vertical motions of the car and counterweight are induced by the building structure motions. When the frequency of the building coincides with the fundamental natural frequency of the ropes, large resonance whirling motions of the ropes result. This phenomenon leads to impacts of the ropes on the elevator walls, large displacements of the car and counterweight making the building and elevator system unsafe. This paper presents a comprehensive mathematical model of a high-rise elevator system taking into account the combined lateral stiffness of the roller guides and guide rails. The results and analysis presented in the paper demonstrate frequency curve veering phenomena and a wide range of resonances that occur in the system. A case study is presented when the car is parked at a landing level where the fundamental natural frequencies of the car, suspension and compensating rope system coincide with one of the natural frequencies of the high-rise building. The results show a range of nonlinear dynamic interactions between the components of the elevator system that play a significant role in the operation of the entire installation.

1. Introduction

Lateral vibrations of the suspension and compensating ropes in a high-rise elevator system are induced by the building motions caused by high winds. In general, a high-rise building has infinite number of natural frequencies, but the main interactions between the ropes and the building structure occur when the first two natural frequencies of the building coincide with the fundamental natural frequencies of the ropes. Then large resonance whirling motions of the ropes then result. This phenomenon causes impact loads in the elevator shaft, leading to adverse dynamic behaviour of the entire elevator system. The impact loads affect the elevator installation resulting in interruptions of service and damage to the components of the system. Furthermore, the car, counterweight and compensating sheave suffer from vertical vibrations due to the coupling with lateral vibrations of the ropes.

The dynamics of ropes and cables has attracted the attention of considerable number of researchers in various types of applications. For example in the context of civil engineering applications the behaviour of cable stayed bridges and guyed towers supported by inclined ropes is studied in [1–3], respectively. In lifting applications the multibody dynamic behaviour of ropes has been studied when heavy cargo is suspended by ropes in a floating crane system [4], and the kinematic and dynamic analysis of rope winding (unwinding) process has been the subject of a study presented in [5]. Another example of engineering applications of ropes is in building elevators and mine hoists [6–9]. The nonlinear modal interactions taking place in a model of an aramid suspension rope system were studied in [10]. The model consisted of an aramid suspension rope, a pulley assembly and a rigid suspended mass. The mathematical model of the system was validated with laboratory tests, the results show the nonlinear couplings may lead to adverse modal interactions in the system. A spatial discretization and substructure method developed in [11] to accurately calculate the dynamic responses a rope system with a time varying length parameter was proposed. The dependent variables of a distributed-parameter component are decomposed into boundary-induced terms and internal terms. In [11] the first part the methodology was developed and in [12] the second part the longitudinal, transverse, and their coupled vibrations of moving elevator cable-car systems is applied with different choices of boundary motions. The effect of longitudinal high frequency excitation which may stiffen a continuous elastic structure is studied in [13]. A structure employing a piano string positioned horizontally is considered and the experimental results demonstrate the validity of the theoretical predictions of the lateral displacements of the string.

The vibration analysis of a vertical rope of changing length and the application of the multiple time scales method to develop approxi-

* Corresponding authors.
E-mail addresses: rsc7@nyu.edu (R.S. Crespo), stefan.kaczmarczyk@northampton.ac.uk (S. Kaczmarczyk).

https://doi.org/10.1016/j.ijmecsci.2018.01.011
Received 4 March 2017; Received in revised form 26 October 2017; Accepted 10 January 2018
Available online 11 January 2018

Nomenclature

$A_{V/W}$	displacement amplitudes in the lateral in plane and out of plane directions
a_1	flange width of guide rail T cross section
a_2	web height of guide rail T cross section
a_3	thickness of guide rail T cross section
b_1	distance measured from the bottom landing level to the centre of the compensating sheave
b_2	distance measured from the centre of the traction sheave to the centre of the diverter pulley
c_{in}	generalised coordinates in the lateral out of plane direction of the ith rope
$D_{irn}{}^{V/W}$	coefficients that account for the quadratic nonlinear coupling of the system of the ith rope in the lateral in plane and out of plane directions
E_G	modulus of elasticity of the guide rail
EA_i	product of the modulus of elasticity and the cross-sectional area the ith rope
$F_{ir}{}^{V/W}$	excitation for the lateral in plane and out of plane direction
F_{CR}, F_{CS}, F_{CW}	excitation forces acting on the elevator car, compensating sheave, and counterweight
h_0	height from the bottom landing level to the centre of the traction sheave
h_t	position of the elevator car
h_{trav}	height of travel
$J_{y/z}$	moment of inertia of the cross-sectional area of the guide rail in the lateral in plane and out of plane direction
$K_G{}^{V/W}$	combined stiffness of the guide rails in the lateral in plane and out of plane direction
K_c	stiffness of the elevator car suspension-tyre system
$k_{irn}{}^{V/W}$	coefficients that account for the lateral in plane and out of plane linear stiffness of rope ith
$k_{1/2}$	equivalent spring constant that represents the combined stiffness of the car suspension, tyre and guide rail system for the in plane and out of plane motion
k^{u1}, $\bar{k}^{u2}$, $\hat{k}^{u2}$	coefficients that account for the longitudinal linear stiffness of the elevator car, compensating sheave, and counterweight
k^{u2}, $\bar{k}^{u1}$, $\hat{k}^{u1}$	coefficients corresponding to the linear coupling between the longitudinal displacements of the elevator car, compensating sheave, and counterweight
${k_n}^{u3}$, ${k_n}^{u4}$	coefficients in the lateral in plane and out of plane direction that account for the linear coupling terms between the longitudinal displacements of the elevator car
$\bar{k}_n{}^{u4}$, $\bar{k}_n{}^{u5}$	coefficients in the lateral in plane and out of plane direction that account for the linear coupling terms between the longitudinal displacements of the compensating sheave
L_i	rope length of the ith rope
L_G	length of the guide rail section
m_i	mass per unit length of the ith rope
$M_{1/2/3}$	mass of the elevator car, compensating sheave, and counterweight
n_1, n_2	number of suspension and compensating ropes
N	number of the lateral in plane and out of plane modes
q_{in}	generalized coordinates in the lateral in plane direction
$R^{V1/W1}{}_{irnjp}$, $R^{V2/W2}{}_{irnjp}$	coefficients corresponding to the cubic nonlinear coupling of the system for the ith rope for the lateral in plane and out of plane direction
$R^{u1/u2}$, $\bar{R}^{u1/u2/u3/u4}$, $\hat{R}^{u1/u2/u3/u4}$	coefficients that account for the lateral in plane and out of plane quadratic nonlinear terms acting in the longitudinal direction of the elevator car, compensating sheave, and counterweight
$S_{V/W}$	kinematic excitation functions in the lateral in plane and out of plane directions
t	time
T_i	tension of the ith rope
U_{CR}, U_{CS}, U_{CW}	dynamic displacements in the longitudinal direction of the elevator car, compensating sheave and counterweight
U_i	dynamic displacement in the longitudinal direction of rope ith
V_{CR}	dynamic displacement in the lateral in plane direction of the elevator car
V_i	dynamic displacement in the lateral in plane direction of the ith rope
$\bar{V}_i$	elastic deformations measured relative to the building motion in the lateral in plane direction of the ith rope
W_{CR}	dynamic displacement in the lateral out of plane direction of the elevator car

W_i	dynamic displacement in the lateral out of plane direction of the *i*th rope
$\bar{W}_i$	elastic deformations relative to the building motion in the lateral out of plane direction of the *i*th rope
x_i	Eulerian spatial coordinate of the *i*th rope

Greek symbols

α_{in}	normal free oscillation modes of the corresponding linear undamped stationary components in the lateral out of plane direction
${\beta_{1n}}^{V/W}$, ${\beta_{2n}}^{V/W}$	eigenvalues in lateral in plane and lateral out of plane direction for the suspension and compensating ropes at the car side
ε	Green's strain measure
${\zeta_{ir}}^{V/W}$	modal damping ratio in the lateral in plane and out of plane direction of the *i*th rope
$\zeta_1, \zeta_2, \zeta_3$	modal damping ratio in the longitudinal direction
ξ	lateral displacements of the structure corresponding to the top of the building at the machine room level and to the position of the elevator car and counterweight
ϕ_{in}	normal free oscillation modes of the corresponding linear undamped stationary components in the lateral in plane direction
ψ	shape function related to the fundamental mode of the host building structure
$\Omega_{V/W}$	frequency of kinematic excitation in the lateral in plane direction and the lateral out of plane direction, respectively
${\omega_r}^{V(i)/W(i)}$	undamped lateral in plane and out of plane natural frequencies of rope *i*th
$\omega_{1/2/3}$	longitudinal natural frequencies of the vertical responses

mate solutions to demonstrate the dynamical behaviour of a rope system was analysed in [14]. It was demonstrated that the Galerkin truncation method cannot be applied to obtain asymptotic results on long timescales.

A small bending stiffness relative to tension was included in the mathematical models for stationary and moving hoist ropes studied in [15] and the convergence of the models were examined.

High-rise elevator systems are composed of mechanical components that interact with each other when the elevator car is stationary or in motion. The previous research was focused on specific parts or sections of the elevator system to better understand the dynamical behaviour of each component. For example, in [16] the vertical vibrations of the compensating sheave suspended by compensating ropes has been analysed. A mathematical model is developed to evaluate the vertical motion of the compensating sheave during different emergency scenarios such as the brake activation and buffer strike to determine the maximum vertical displacement of the compensating sheave. In [17] the longitudinal vibrations of a suspension rope are studied with a car frame attached to the bottom end of the rope, when the top end of the rope is fixed to the upper support. Different case studies were considered to understand the longitudinal dynamic behaviour of the suspension ropes coupled with the elevator car assembly when the system is stationary. In [18] the vertical vibrations are analysed by a five degree of freedom lumped parameter model representing the car, compensating sheave, and counterweight with the machine drive system and controllers used in the laboratory experimental tests. In [19] the lateral vibrations of the compensating ropes due to the longitudinal vibrations of the compensating sheave and the rope winding shape around the compensating sheave are studied by developing a lumped mass-spring model to compare with experimental results. In [20] a simplified calculation method based on a single degree of freedom system to predict the lateral displacements of the suspension and compensating ropes has been developed. The simplified model was compared with a finite difference method which considers the building structure lateral displacements and the ground displacement as inputs.

A high-rise elevator system includes long slender continua such as ropes and cables that are linked with discrete mass/inertia elements. In the dynamic analysis they can be represented as beam or string elements. An analysis of elastic beams with concentrated masses and spring supports was conducted in [21,22]. In [21] the mode shape function and frequency equation were derived for cantilever beams with lumped masses and spring supports in different configurations. In [22] a static and dynamic stability analysis of a laminated composite cantilever beam supported by a system comprising a combination of linear translational spring and torsional spring excited by axial forcing has been carried out. Research concerning the subject of non-linear vibrations of axially moving material was studied in [23]. In this work a non-linear axially moving cable coupled with the lateral displacements has been considered. The response of the system has been studied in the region of a 3:1 internal resonance between the first two lateral modes. The analysis of transverse vibration of an axially moving finite length beam where two points are supported by rotating rollers is presented in [24]. The results show that the modal exchanges occur at the veering regions of the natural frequency loci. The dynamic model includes the translational and rotational motions as well as the deflection of the moving beam. In [25] a model of an axially moving cable of constant length is developed. In this work the cable is excited by forced vibration applied at the supports. This scenario is relevant to moving walks or belts systems. When both ends are excited in phase, the symmetric and asymmetric mode shows the resonance phenomena caused by the effect of motion. In [26] a model is developed consisting of a power transmission belt system excited by pulleys having an eccentricity. The experimental results showed a range of response amplitudes and near resonance amplitude jumps.

The application of active roller guides in a high rise elevator system to mitigate the effects of lateral excitations acting upon a car due to irregularities of the guiding system [27,28] is considered in [29]. Active roller guides apply forces in the opposite direction to the lateral motion in order to maintain the roller guides being always in contact with the guide rails [30]. The implementation of roller guides in high-rise elevator system improves ride quality of passengers in the elevator car. The study presented in [31] investigates a deterministic and stochastic model of a cable – mass system with an auxiliary mass to act as a transverse tuned mass damper to mitigate the rope displacements when the length of the cable varies slowly.

Coupled vibrations of buildings and elevator ropes with a focus on the analysis of the car side are studied in [32]. An experimental test rig is used to validate the results predicted from the theoretical model. The proposed model is based on a real building site and the elevator rope data corresponding to the Hyundai Asan elevator tower, located in Icheon, South Korea, are used to predict the response of the system. An overview provided in [33] shows a case study of the One World Trade Center site, New York, USA. The One World Trade Center building is 541.0 m tall and vertical transportation is provided by a total of 73 elevators of which ten elevators travel directly from the ground floor level to the roof level.

This paper extends the analysis presented in the previous research to develop a comprehensive mathematical model of a high-rise elevator system in order, to understand and to predict the interaction between the lateral vibrations of the suspension and compensating ropes coupled with the longitudinal vibrations of the elevator car, compensating sheave, and counterweight taking into account the combined lateral stiffness characteristics of the elevator car guiding system. Additionally,

the results presented in this paper demonstrate the effects of the veering regions of the natural frequency loci in the lateral in plane and out of plane direction of the elevator car, suspension and compensating ropes subsystem. The Hamilton Principle [34] is used to derive the model which can then be used in the design and analysis of a high-rise elevator systems to predict the lateral displacements of the ropes and the longitudinal displacements of the elevator car, compensating sheave and counterweight. The prediction can then inform the development of relevant mitigating strategies to minimize the effects of excessive vibrations and to improve ride quality.

A scenario is discussed when the car is parked at the height level at which the fundamental natural frequencies of the suspension and compensating ropes at the car side become near each other with a comparison of the high and low lateral stiffness of the roller guide – suspension-tyre and guide rail system. The dynamic response of the system when the building is subjected to a low frequency sway in the lateral directions is determined. The results predict a range of nonlinear dynamic interactions between the components of the elevator system that play a significant role in the operation of the entire installation.

2. The mathematical model of an elevator system

In this section, the mathematical model of an elevator system is described and the equations of motion of the complete elevator system are derived and explained.

2.1. Description of the mathematical model

The model of an elevator system with a car of mass M_1, compensating sheave of mass M_2, and counterweight of mass M_3, is depicted in Fig. 1. The suspension and compensating ropes have mass per unit length m_1 and m_2, a product of the modulus of elasticity and the cross-sectional area EA_1 and EA_2, respectively.

The parameter b_1 represents the distance measured from the bottom landing level to the centre of the compensating sheave. The parameter b_2 denotes the distance measured from the centre of the traction sheave to the centre of the diverter pulley and h_0 represents the distance measured from the bottom landing level to the centre of the traction sheave. The parameter h_{trav} is the height of travel of the elevator car. The elevator car, compensating sheave and counterweight are considered as point masses, thus the height is neglected. The parameter h_t is the position of the elevator car measured from the bottom landing level to the elevator car.

The lengths L_1 and L_4 of the suspension ropes and the lengths L_2 and L_3 of the compensating ropes are defined as shown in Fig. 1. The response of the elevator ropes subjected to dynamic loading due to the building sway are represented by the lateral in-plane and lateral out of plane displacements denoted as $V_i(x_i,t)$ and $W_i(x_i,t)$ where the subscript $i=1,2,3,4$ corresponds to the sections of the ropes of length L_1, L_2, L_3, and L_4, respectively. The displacements of the ropes relative to the configuration of the ropes when they are stretched by the structure motion are represented by $\bar{V}_i(x_i,t)$ and $\bar{W}_i(x_i,t)$. The lateral in-plane and lateral out of plane motions of the ropes are coupled with the longitudinal motions of the ropes that are denoted as $U_i(x_i,t)$. The variable x_i is the spatial coordinate of each rope measured from the top support of each rope. The longitudinal motions of the car, compensating sheave and counterweight are denoted as $U_{CR}(t)$, $U_{CS}(t)$, and $U_{CW}(t)$, respectively. The lateral in plane and out of plane motions of the car denoted as $V_{CR}(t)=V_1(L_1,t)=V_2(0,t)$ and $W_{CR}(t)=W_1(L_1,t)=W_2(0,t)$. The lateral motions of the counterweight are not considered in this mathematical model.

More emphasis has been placed on modelling of the car–building interface components due to their effects on ride quality. The compensating sheave and counterweight are restricted to move in the longitudinal direction only.

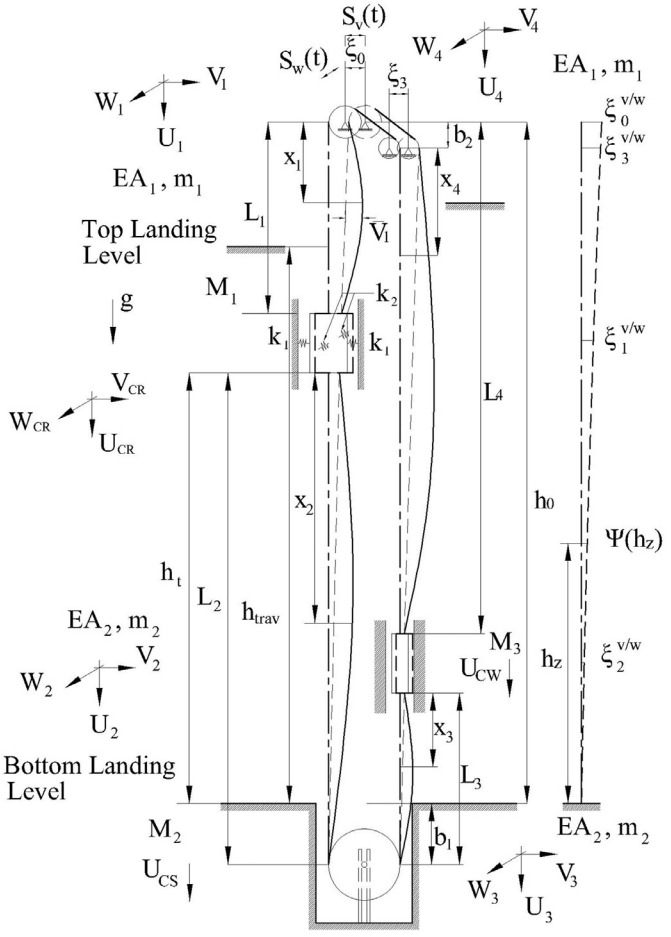

Fig. 1. Model of stationary elevator system, $M_{1/2/3}$ – mass of elevator car, compensating sheave, counterweight, $L_{1/2/3/4}$ – length of suspension and compensating ropes, and $\xi_{0/1/2/3}$ – lateral displacements of the structure at the top of the building measured at different positions (see the definition of all symbols in the Nomenclature).

The parameters k_1 and k_2 represents the combined stiffness of the roller guides and guide rails in the lateral in plane and the lateral out of plane direction, respectively. The roller guide and guide rails form the guiding interface between the building and the elevator car and counterweight. The guiding interface ensures the relative position of the elevator car and counterweight along the height of travel as discussed in [35].

The guide rails are very well secured to the elevator shaft walls to avoid any vibration that may be induced by the dynamic forces when the elevator car is travelling along the hoistway. Each section of the guide rails has a length approximately of 5.00 m. The guide rail system installed in a building shaft can be treated as a multispan beam subjected to lateral loading. The guide rail size is determined by relevant design calculations taking into account the code requirements [36] for the guide rail deflections to satisfy the safety requirements. In the scenario considered in this paper it is assumed that the roller guide applies a constant load F_G at the centre of the span. The guide rail span stiffness can then be calculated by assuming that the span represents a fixed–fixed beam. The stiffness coefficients of the guide rail modelled as massless springs of constants $K_G{}^V$ and $K_G{}^W$ respectively, are then determined as

$$K_G^{V/W} = \frac{192 E_G J_{y/z}}{L_G^3}, \tag{1}$$

where E_G is Young's modulus of elasticity of the guide rail, $J_{y/z}$ is the second moment of inertia of the cross-sectional area of the guide rail in the lateral in plane and out of plane direction and L_G is the length of the

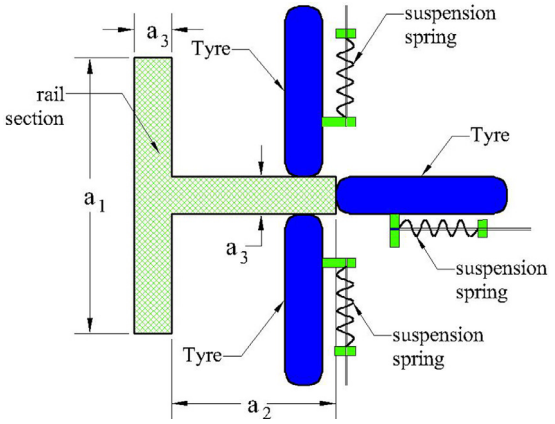

Fig. 2. Roller guide arrangement consisting of a suspension-tyre system and a guide rail section.

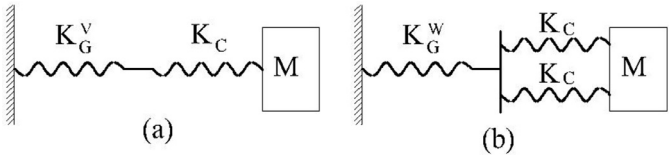

Fig. 3. Combined spring element between the elevator car and guide rail, $K_G{}^{V/W}$ – stiffness coefficients of guide rail and K_c – stiffness of elevator car suspension-tyre system in (a) lateral in plane and (b) lateral out of plane.

guide rail section. The cross section of a guide rail used in the elevator system forms a *T* section. The roller guide arrangement and guide rail cross section are shown in Fig. 2. The flange width, web height, and thickness of the *T* cross section are shown in Fig. 2 as a_1, a_2, and a_3, respectively.

Based on the model used in [37] the total combined stiffness of the roller guide – suspension-tyre and guide rail system can be modelled in the lateral in plane and lateral out of plane directions as shown in Fig. 3(a) and (b), respectively. The total combined stiffness of the system is mostly affected by the stiffness of the elevator car suspension-tyre when using hard or soft tyres, as will be shown in the case study in Section 3.

The parameters k_1 and k_2 can be estimated by using Eqs. (2) and (3). The stiffness of the elevator car suspension-tyre system is represented by K_c.

$$k_1 = \frac{K_G^V K_c}{K_G^V + K_c}, \tag{2}$$

$$k_2 = \frac{2K_G^W K_c}{K_G^W + 2K_c}. \tag{3}$$

The lateral displacements of the structure expressed in terms of the displacements at the top of the building measured at the machine room level and to the position of the car and counterweight are represented as ξ_0, ξ_1, ξ_2, and ξ_3 and are defined in Eqs. (11)–(14). Furthermore, ψ_1, ψ_2, ψ_3, ψ_4, and ψ_5 are non-dimensional coefficients obtained by using the polynomial function $\psi(h_z)$ representing the fundamental mode shape of a cantilever beam, defined in Eq. (4). The shape function is assumed to be related to the fundamental mode of the high-rise building and is approximated by a cubic polynomial representing the lateral displacements of the structure corresponding to the top of the structure and to the position of the car and counterweight estimated by Eqs. (5)–(9).

$$\psi(h_z) = 3\left(\frac{h_z}{h_0}\right)^2 - 2\left(\frac{h_z}{h_0}\right)^3, \tag{4}$$

$$\psi_1 = 3\left(1 - \frac{L_1}{h_0}\right)^2 - 2\left(1 - \frac{L_1}{h_0}\right)^3, \tag{5}$$

$$\psi_2 = 3\left(\frac{L_2 - b_1}{h_0}\right)^2 - 2\left(\frac{L_2 - b_1}{h_0}\right)^3, \tag{6}$$

$$\psi_3 = 3\left(\frac{L_3 - b_1}{h_0}\right)^2 - 2\left(\frac{L_3 - b_1}{h_0}\right)^3, \tag{7}$$

$$\psi_4 = 3\left(1 - \frac{L_4 + b_2}{h_0}\right)^2 - 2\left(1 - \frac{L_4 + b_2}{h_0}\right)^3, \tag{8}$$

$$\psi_5 = 3\left(1 - \frac{b_2}{h_0}\right)^2 - 2\left(1 - \frac{b_2}{h_0}\right)^3. \tag{9}$$

The quantities $S_V(t)$ and $S_W(t)$ represent the displacements of the building at the machine room level in the lateral in plane and out of plane directions, respectively, and are expressed by the following equation:

$$S_{V/W} = A_{V/W} \sin\left(\Omega_{V/W} t\right). \tag{10}$$

The displacement amplitudes in the lateral in plane and out of plane directions are represented as A_V and A_W. The external frequency of excitation lateral in plane and out of plane direction are represented as Ω_V and Ω_W. According to Fig. 1 the lateral displacements $\xi_0{}^W$, $\xi_0{}^W$, $\xi_1{}^V$, $\xi_1{}^W$, $\xi_2{}^V$, $\xi_2{}^W$, $\xi_3{}^V$, and $\xi_3{}^W$ in the lateral in plane and out of plane direction and the non-dimensional coefficients from the shape functions ψ_1, ψ_2, ψ_3, ψ_4, and ψ_5 are related as shown in the following equations:

$$\xi_0^{V/W} = S_{V/W}, \tag{11}$$

$$\xi_1^{V/W} = \psi_1 S_{V/W} = \psi_2 S_{V/W}, \tag{12}$$

$$\xi_2^{V/W} = \psi_3 S_{V/W} = \psi_4 S_{V/W}, \tag{13}$$

$$\xi_3^{V/W} = \psi_5 S_{V/W}. \tag{14}$$

The following assumptions are made. The ropes are treated as uniform strings. The product of the modulus of elasticity and the cross-sectional area *EA* of the ropes are considered constant. The bending stiffness of all ropes is neglected, due to the criterion $EI/TL^2 << 1$ according to Zhu and Ren [11], where *EI* represents the product of the modulus of elasticity and the second moment of inertia of the cross-sectional area of the rope, *T* corresponds to the tension of the rope, and *L* represents the length of the rope. This can be done because the bending stiffness have small effect when the ropes have long lengths. The multi-rope system is represented by one equivalent rope, thus no interactions between the ropes are accounted for in the mathematical model. The elevator car, compensating sheave, and counterweight are treated as concentrated mass elements. It is assumed that the elevator system dynamics does not affect the dynamics of the building structure. The lateral damping characteristics of the suspension and compensating ropes in all modes is represented by the modal damping ratios. The longitudinal damping of the elevator car, compensating sheave, and counterweight are represented by longitudinal damping ratios.

The elastic Green's strain measure of the *i*th rope expressed by the following equation:

$$\varepsilon_i = U_{ix} + \frac{1}{2}\left(V_{ix}^2 + W_{ix}^2\right), \tag{15}$$

where the subscript *x* denotes the partial derivative with respect to the spatial coordinate. The coupling between the suspension and compensating ropes at the car side due to the constraints at the elevator car by the springs k_1 and k_2 in both lateral in plane and out of plane directions are considered. The elastic interface with the building at the counterweight side is neglected. The model represents a typical scenario when the elevator car is positioned at a given height in the shaft and the electromechanical brake is applied at the machine.

2.2. Derivation of the accurate mathematical model

The Hamilton Principle to derive the equations of motion of the system is stated as,

$$\int_{t_1}^{t_2} \left(\delta\hat{Q} - \delta\Pi + \delta W_{nc}\right) dt = 0, \tag{16}$$

where $\hat{Q}$, Π and W_{nc} denote the kinetic energy, the potential energy and the work due to non-conservative forces acting upon the system, respectively. The model is considered conservative when is derived, thus work done by the nonconservative forces is neglected between t_1 and t_2 which are the initial and final time. The virtual work of the nonconservative forces in this mathematical model represents the virtual work of damping forces which are introduced later on as linear modal damping ratios.

The boundary conditions are as follows:

$$V_1(0,t) = \xi_0^V, \tag{17}$$

$$W_1(0,t) = \xi_0^W, \tag{18}$$

$$U_1(0,t) = V_2(L_2,t) = W_2(L_2,t) = V_3(L_3,t) = W_3(L_3,t) = U_4(0,t) = 0, \tag{19}$$

$$U_1(L_1,t) = U_2(0,t) = U_{CR}, \tag{20}$$

$$V_1(L_1,t) = V_2(0,t), \tag{21}$$

$$W_1(L_1,t) = W_2(0,t), \tag{22}$$

$$U_2(L_2,t) = U_3(L_3,t) = U_{CS}, \tag{23}$$

$$V_3(0,t) = V_4(L_4,t) = \xi_2^V, \tag{24}$$

$$W_3(0,t) = W_4(L_4,t) = \xi_2^W, \tag{25}$$

$$U_3(0,t) = U_4(L_4,t) = U_{CW}, \tag{26}$$

$$V_4(0,t) = \xi_3^V, \tag{27}$$

$$W_4(0,t) = \xi_3^W. \tag{28}$$

After applying Hamilton Principle the nonlinear equations of motion (29)–(36) are derived, where the subscript t represents the partial derivative with respect to time. The Eqs. (29)–(31) describe the dynamics of the ith rope in the elevator system, where $i=1,2,3,4$.

$$m_i V_{itt} - T_{ix}V_{ix} - EA_i\left(U_{ix} + \frac{1}{2}\left(V_{ix}^2 + W_{ix}^2\right)\right)_x V_{ix} - T_i V_{ixx} - EA_i\left(U_{ix} + \frac{1}{2}\left(V_{ix}^2 + W_{ix}^2\right)\right)V_{ixx} = 0, \tag{29}$$

$$m_i W_{itt} - T_{ix}W_{ix} - EA_i\left(U_{ix} + \frac{1}{2}\left(V_{ix}^2 + W_{ix}^2\right)\right)_x W_{ix} - T_i W_{ixx} - EA_i\left(U_{ix} + \frac{1}{2}\left(V_{ix}^2 + W_{ix}^2\right)\right)W_{ixx} = 0, \tag{30}$$

$$m_i U_{itt} - T_{ix} - EA_i\left(U_{ix} + \frac{1}{2}\left(V_{ix}^2 + W_{ix}^2\right)\right)_x - m_i g = 0. \tag{31}$$

The Eqs. (32) and (33) represent the boundary conditions at $x_1 = L_1$ for the lateral in plane and lateral out of plane motions.

$$M_1 V_{1tt}(L_1,t) + \left(T_1(x) + EA_1\left(U_{1x} + \frac{1}{2}\left(V_{1x}^2 + W_{1x}^2\right)\right)\Big|_{x_1=L_1}\right)V_{1x}|_{x_1=L_1} - \left(T_2(x) + EA_2\left(U_{2x} + \frac{1}{2}\left(V_{2x}^2 + W_{2x}^2\right)\right)\Big|_{x_2=L_2}\right) V_{2x}|_{x_2=0} + 2k_1 V_1(L_1,t) - 2k_1\xi_1^v = 0, \tag{32}$$

$$M_1 W_{1tt}(L_1,t) + \left(T_1(x) + EA_1\left(U_{1x} + \frac{1}{2}\left(V_{1x}^2 + W_{1x}^2\right)\right)\Big|_{x_1=L_1}\right)W_{1x}|_{x_1=L_1} - \left(T_2(x) + EA_2\left(U_{2x} + \frac{1}{2}\left(V_{2x}^2 + W_{2x}^2\right)\right)\Big|_{x_2=L_2}\right) W_{2x}|_{x_2=0} + 2k_2 W_1(L_1,t) - 2k_2\xi_1^w = 0. \tag{33}$$

The Eqs. (34)–(36) are the boundary conditions at $x_1 = L_1$ and $x_2 = 0$, $x_2 = L_2$ and $x_3 = L_3$, $x_3 = 0$, and $x_4 = L_4$ in the longitudinal direction for the elevator car, compensating sheave, and counterweight, respectively.

$$M_1(U_{CR})_{tt} + T_1(L_1) + EA_1\left(U_{1x} + \frac{1}{2}\left(V_{1x}^2 + W_{1x}^2\right)\right)\Big|_{x=L_1} - T_2(0) - EA_2\left(U_{2x} + \frac{1}{2}\left(V_{2x}^2 + W_{2x}^2\right)\right)\Big|_{x=0} - M_1 g = 0, \tag{34}$$

$$M_2(U_{CS})_{tt} + T_2(L_2) + EA_2\left(U_{2x} + \frac{1}{2}\left(V_{2x}^2 + W_{2x}^2\right)\right)\Big|_{x=L_2} + T_3(L_3) + EA_2\left(U_{3x} + \frac{1}{2}\left(V_{3x}^2 + W_{3x}^2\right)\right)\Big|_{x=L_3} - M_2 g = 0, \tag{35}$$

$$M_3(U_{CW})_{tt} + T_4(L_4) + EA_1\left(U_{4x} + \frac{1}{2}\left(V_{4x}^2 + W_{4x}^2\right)\right)\Big|_{x=L_4} - T_3(0) - EA_2\left(U_{3x} + \frac{1}{2}\left(V_{3x}^2 + W_{3x}^2\right)\right)\Big|_{x=0} - M_3 g = 0. \tag{36}$$

The mean quasi static rope tensions are derived by balance of forces (see Fig. 1) which are represented by Eqs. (37)–(40), where g is the acceleration of gravity (9.81 m/s^2).

$$T_1(x_1) = \left(M_1 + m_1(L_1 - x) + m_2 L_2 + \frac{M_2}{2}\right)g, \tag{37}$$

$$T_2(x_2) = \left(\frac{M_2}{2} + m_2(L_2 - x_2)\right)g, \tag{38}$$

$$T_3(x_3) = \left(\frac{M_2}{2} + m_2(L_3 - x_3)\right)g, \tag{39}$$

$$T_4(x_4) = \left(M_3 + m_1(L_4 - x_4) + m_2 L_3 + \frac{M_2}{2}\right)g. \tag{40}$$

The overall lateral in plane displacements of each rope can be represented by the following equations:

$$V_1(x_1,t) = \bar{V}_1(x_1,t) + S_V\left(1 + (\psi_1 - 1)\frac{x_1}{L_1}\right), \tag{41}$$

$$V_2(x_2,t) = \bar{V}_2(x_2,t) + S_V\psi_2\left(1 - \frac{x_2}{L_2}\right), \tag{42}$$

$$V_3(x_3,t) = \bar{V}_3(x_3,t) + S_V\psi_3\left(1 - \frac{x_3}{L_3}\right), \tag{43}$$

$$V_4(x_4,t) = \bar{V}_4(x_4,t) + S_V\left(\psi_5 + (\psi_4 - \psi_5)\frac{x_4}{L_4}\right). \tag{44}$$

where $V_i(x_i,t)$ are the overall response of the elevator ropes in the lateral in plane direction subjected to dynamic loading due to the building sway where the subscript $i=1,2,3,4$ corresponds to the rope ith. The displacements of the ropes relative to the configuration of the ropes when they are stretched by the structure motion are represented by $\bar{V}_i(x_i,t)$. The second term in Eqs. (41)–(44) are the stretch of rope ith due to the deformation of the structure. Similarly, the overall lateral out of plane displacements of each rope can be expressed by the application of similar transformations. The partial derivative with respect to x and t can be derived and replaced into Eq. (31) resulting in Eq. (45).

$$m_i U_{itt} - EA_i\left(U_{ix} + \frac{1}{2}\left(V_{ix}{}^2 + W_{ix}{}^2\right)\right)_x = 0. \tag{45}$$

According to Kaczmarczyk and Picton [6], the longitudinal natural frequencies of steel wire ropes are much higher than their lateral natural frequencies, thus the inertia of the ropes in the longitudinal direction can be neglected, resulting in the following equation:

$$EA_i\left(U_{ix} + \frac{1}{2}\left(V_{ix}{}^2 + W_{ix}{}^2\right)\right)_x = 0, \text{for } i = 1,2,3,4 \tag{46}$$

Thus, the following results

$$U_{ix} + \frac{1}{2}\left(V_{ix}{}^2 + W_{ix}{}^2\right) = e_i(t), \text{for } i = 1,2,3,4 \tag{47}$$

where $e_i(t)$ is an arbitrary function which depends on the boundary conditions. Substituting Eq. (47) into Eq. (29)–(36) gives:

$$m_i V_{itt} + T_{ix}V_{ix} - T_i V_{ixx} - EA_i e_i(t)V_{ixx} = 0, \tag{48}$$

$$m_i W_{itt} + T_{ix}W_{ix} - T_i W_{ixx} - EA_i e_i(t)W_{ixx} = 0, \tag{49}$$

$$\begin{aligned} &M_1\bar{V}_1(L_1,t)_{tt} - M_1\xi_1^V\lambda_v^2 + T_1(L_1)\bar{V}_{1x} - T_1(L_1)\frac{\left(\xi_1^V - S_V\right)}{L_1} \\ &\quad + EA_1e_1(t)\bar{V}_{1x} - EA_1e_1(t)\frac{\left(\xi_1^V - S_V\right)}{L_1} \\ &-T_2(0)\bar{V}_{2x} + T_2(0)\frac{\xi_1^V}{L_2} + EA_2e_2(t)\bar{V}_{2x} - EA_2e_2(t)\frac{\xi_1^V}{L_2} \\ &\quad + 2k_1\bar{V}_1(L_1,t) = 0 \end{aligned}, \tag{50}$$

$$\begin{aligned} &M_1\bar{W}_1(L_1,t)_{tt} - M_1\xi_1^W\lambda_W^2 + T_1(L_1)\bar{W}_{1x} - T_1(L_1)\frac{\left(\xi_1^W - S_W\right)}{L_1} \\ &\quad + EA_1e_1(t)\bar{W}_{1x} - EA_1e_1(t)\frac{\left(\xi_1^W - S_W\right)}{L_1} \\ &-T_2(0)\bar{W}_{2x} + T_2(0)\frac{\xi_1^W}{L_2} + EA_2e_2(t)\bar{W}_{2x} - EA_2e_2(t)\frac{\xi_1^W}{L_2} \\ &\quad + 2k_1\bar{W}_1(L_1,t) = 0 \end{aligned}, \tag{51}$$

$$M_1(U_{CR})_{tt} + T_1(L_1) + EA_1e_1(t) - T_2(0) - EA_2e_2(t) - M_1g = 0, \tag{52}$$

$$M_2(U_{CS})_{tt} + T_2(L_2) + EA_2e_2(t) + T_3(L_3) + EA_2e_3(t) - M_2g = 0, \tag{53}$$

$$M_3(U_{CW})_{tt} + T_4(L_4) + EA_1e_4(t) - T_3(0) - EA_2e_3(t) - M_3g = 0. \tag{54}$$

The boundary conditions at $x_i=0$, L_i for $i=3$, 4, $x_1=0$ and $x_2=L_2$ are $\bar{V}_i(x_i,t)=\bar{W}_i(x_i,t)=0$ (are trivial). The boundary conditions at $x_1=L_1$ and $x_2=0$ satisfy $\bar{V}_1(x_1,t)=\bar{V}_2(x_2,t)$ and $\bar{W}_1(x_1,t)=\bar{W}_1(x_2,t)$ are represented by the equations of motion of the car mass in the lateral in plane and out of plane direction. The linear natural modes of the lateral in plane and lateral out of plane motions for the suspension rope at the car side (rope 1) are given as

$$\phi_{1n}(x_1) = \sin\left(\beta_{1n}^V x_1\right), \tag{55}$$

$$\alpha_{1n}(x_1) = \sin\left(\beta_{1n}^W x_1\right). \tag{56}$$

The linear natural modes of the lateral in plane and lateral out of plane motion for the compensating rope at the car side (rope 2) are represented by the following equations:

$$\phi_{2n}(x_2) = \sin\beta_{1n}^V L_1\cos\beta_{2n}^V x_2 - \frac{\sin\beta_{1n}^V L_1\cos\beta_{2n}^V L_2}{\sin\beta_{2n}^V L_2}\sin\beta_{2n}^V x_2, \tag{57}$$

$$\alpha_{2n}(x_2) = \sin\beta_{1n}^W L_1\cos\beta_{2n}^W x_2 - \frac{\sin\beta_{1n}^W L_1\cos\beta_{2n}^W L_2}{\sin\beta_{2n}^W L_2}\sin\beta_{2n}^W x_2, \tag{58}$$

where ${\beta_{1n}}^V$, ${\beta_{2n}}^V$, ${\beta_{1n}}^W$, and ${\beta_{2n}}^W$ are the lateral in plane and lateral out of plane eigenvalues for the suspension and compensating ropes at the car side, respectively, given in terms of the natural frequencies. The natural frequencies of the lateral in plane and out of plane directions of both ropes can be obtained from the following equation:

$$\begin{aligned} &\omega^{V/W}\sqrt{T_2m_2}\cos\left(\omega^{V/W}L_2\sqrt{\tfrac{m_2}{L_2}}\right)\sin\left(\omega^{V/W}L_1\sqrt{\tfrac{m_1}{L_1}}\right) \\ &+2k_{1/2}\sin\left(\omega^{V/W}L_2\sqrt{\tfrac{m_2}{L_2}}\right)\sin\left(\omega^{V/W}L_1\sqrt{\tfrac{m_1}{L_1}}\right) \\ &+\omega^{V/W}\sqrt{T_1m_1}\sin\left(\omega^{V/W}L_2\sqrt{\tfrac{m_2}{L_2}}\right)\cos\left(\omega^{V/W}L_1\sqrt{\tfrac{m_1}{L_1}}\right) \\ &-M_1\left(\omega^{V/W}\right)^2\sin\left(\omega^{V/W}L_2\sqrt{\tfrac{m_2}{L_2}}\right)\sin\left(\omega^{V/W}L_1\sqrt{\tfrac{m_1}{L_1}}\right) = 0 \end{aligned}. \tag{59}$$

The corresponding eigenvalues can then be determined from the following equation:

$$\beta_{in}^{V/W} = \omega_n^{V/W}\sqrt{\frac{m_i}{T_i}}, \text{for } i = 1 \text{ and } 2 \tag{60}$$

On the other hand, at the counterweight side, the linear natural modes of the lateral in plane and lateral out of plane motion are given by the following equation:

$$\alpha_{in} = \phi_{in} = \sin\left(\frac{n\pi}{L_i}x\right), \text{for } i = 3 \text{ and } 4 \tag{61}$$

The corresponding natural frequencies in the lateral in plane and out of plane direction are then determined by the following equation:

$$\omega_n^{V(i)} = \omega_n^{W(i)} = \frac{n\pi}{L_i}\sqrt{\frac{T_i}{m_i}}. \tag{62}$$

2.3. Derivation of the approximate mathematical model

The equations of motion (48)–(54) can be discretized by applying the Galerkin method. In this procedure, the dynamic response of the system is approximated, in the lateral in plane and lateral out of plane directions by the following expansions:

$$\bar{V}_i(x_i,t) = \sum_{n=1}^{N}\phi_{in}(x_i)q_{in}(t), \tag{63}$$

$$\bar{W}_i(x_i,t) = \sum_{n=1}^{N}\alpha_{in}(x_i)c_{in}(t), \tag{64}$$

where $i=1,2,3,4$, $q_{in}(t)$ and $c_{in}(t)$ represent the generalized (modal) coordinates. For the suspension and compensating ropes at the car side the time dependent functions are $q_{1n}(t)=q_{2n}(t)=q_n(t)$ and $c_{1n}(t)=c_{2n}(t)=c_n(t)$ is used. Substituting expansions (63) and (64) into Eq. (47) results in the following equations:

$$\begin{aligned} e_1(t) = {} & \tfrac{U_{CR}}{L_1} + \tfrac{1}{2L_1}\sum_{j=1}^{N}\sum_{p=1}^{N}G_{jp}^{V1}q_j(t)q_p(t) + \tfrac{\xi_1^V - S_V}{L_1^2}\sum_{j=1}^{N}q_j(t)\sin\left(\beta_{1j}^V L_1\right) + \tfrac{\left(\xi_1^V - S_V\right)^2}{2L_1^2} \\ & + \tfrac{1}{2L_1}\sum_{j=1}^{N}\sum_{p=1}^{N}G_{jp}^{W1}c_j(t)c_p(t) + \tfrac{\xi_1^W - S_W}{L_1^2}\sum_{j=1}^{N}c_j(t)\sin\left(\beta_{1j}^W L_1\right) + \tfrac{\left(\xi_1^W - S_W\right)^2}{2L_1^2} \end{aligned}, \tag{65}$$

$$\begin{aligned} e_2(t) = {} & \tfrac{U_{CS} - U_{CR}}{L_2} + \tfrac{1}{2L_2}\sum_{j=1}^{N}\sum_{p=1}^{N}G_{jp}^{V2}q_j(t)q_p(t) + \tfrac{\xi_1^V}{L_2^2}\sum_{j=1}^{N}q_j(t)\sin\left(\beta_{2j}^V L_2\right) + \tfrac{\left(\xi_1^V\right)^2}{2L_2^2} \\ & + \tfrac{1}{2L_2}\sum_{j=1}^{N}\sum_{p=1}^{N}G_{jp}^{W2}c_j(t)c_p(t) + \tfrac{\xi_1^W}{L_2^2}\sum_{j=1}^{N}c_j(t)\sin\left(\beta_{2j}^W L_2\right) + \tfrac{\left(\xi_1^W\right)^2}{2L_2^2} \end{aligned}, \tag{66}$$

$$\begin{aligned} e_3(t) = {} & \frac{U_{CS} - U_{CW}}{L_3} + \frac{1}{4}\sum_{j=1}^{N}\left(\frac{j\pi}{L_3}\right)^2 q_{3j}^2(t) + \frac{\left(\xi_2^V\right)^2}{2L_3^2} \\ & + \frac{1}{4}\sum_{j=1}^{N}\left(\frac{j\pi}{L_3}\right)^2 c_{3j}^2(t) + \frac{\left(\xi_2^W\right)^2}{2L_3^2}, \end{aligned} \tag{67}$$

$$e_4(t) = \frac{U_{CW}}{L_4} + \frac{1}{4}\sum_{j=1}^{N}\left(\frac{j\pi}{L_4}\right)^2 q_{4j}^2(t) + \frac{\left(\xi_2^V - \xi_3^V\right)^2}{2L_4^2} + \frac{1}{4}\sum_{j=1}^{N}\left(\frac{j\pi}{L_4}\right)^2 c_{4j}^2(t) + \frac{\left(\xi_2^W - \xi_3^W\right)^2}{2L_4^2}, \tag{68}$$

where $G_{jp}{}^{V1}$ and $G_{jp}{}^{V2}$ are defined by Eqs. (A.1) and (A.2) are coefficients corresponding to the in plane modes, where $G_{jp}{}^{W1}$ and $G_{jp}{}^{W2}$ are coefficients corresponding to the out of plane modes which can be similarly derived. Substituting expansions (63) and (64) into (48)–(54) applying the orthogonality conditions with respect to the linear modes a system of nonlinear ordinary differential equations shown in Eqs. (69)–(75). The Eqs. (69) and (70) correspond to the lateral in plane and out of plane motion at the car side composed of the suspension ropes, compensating ropes, and elevator car.

$$\begin{aligned}
&\ddot{q}_r(t) + 2\zeta_r^V \omega_r^V \dot{q}_r(t) + \left(\omega_r^V\right)^2 q_r(t) + \sum_{n=1}^{N} k_{rn}^{V1} q_n(t) + k_r^{V3} U_{CR} \\
&\quad + k_r^{V4} U_{CS} + \sum_{n=1}^{N} k_{rn}^{V2} c_n(t) \\
&+ \sum_{n=1}^{N}\sum_{j=1}^{N} D_{rn}^{V1} q_j(t) q_n(t) + \sum_{n=1}^{N}\sum_{j=1}^{N} D_{rn}^{V2} c_j(t) q_n(t) + \sum_{n=1}^{N}\sum_{j=1}^{N} D_{rn}^{V3} c_j(t) c_n(t), \\
&+ \sum_{n=1}^{N}\left(D_{rn}^{V4} U_{CR} + D_{rn}^{V5} U_{CS}\right) q_n(t) + \sum_{n=1}^{N}\sum_{j=1}^{N}\sum_{p=1}^{N} R_{rnjp}^{V1} q_j(t) q_p(t) q_n(t) \\
&+ \sum_{n=1}^{N}\sum_{j=1}^{N}\sum_{p=1}^{N} R_{rnjp}^{V2} c_j(t) c_p(t) q_n(t) + F_r^V = 0
\end{aligned} \tag{69}$$

$$\begin{aligned}
&\ddot{c}_r(t) + 2\zeta_r^W \omega_r^W \dot{c}_r(t) + \left(\omega_r^W\right)^2 c_r(t) + \sum_{n=1}^{N} k_{rn}^{W1} c_n(t) + k_r^{W3} U_{CR} \\
&\quad + k_r^{W4} U_{CS} + \sum_{n=1}^{N} k_{rn}^{W2} q_n(t) \\
&+ \sum_{n=1}^{N}\sum_{j=1}^{N} D_{rn}^{W1} q_j(t) c_n(t) + \sum_{n=1}^{N}\sum_{j=1}^{N} D_{rn}^{W2} c_j(t) c_n(t) + \sum_{n=1}^{N}\sum_{j=1}^{N} D_{rn}^{W3} q_j(t) q_n(t). \\
&+ \sum_{n=1}^{N}\left(D_{rn}^{W4} U_{CR} + D_{rn}^{W5} U_{CS}\right) c_n(t) + \sum_{n=1}^{N}\sum_{j=1}^{N}\sum_{p=1}^{N} R_{rnjp}^{W1} q_j(t) q_p(t) c_n(t) \\
&+ \sum_{n=1}^{N}\sum_{j=1}^{N}\sum_{p=1}^{N} R_{rnjp}^{W2} c_j(t) c_p(t) c_n(t) + F_r^W = 0
\end{aligned} \tag{70}$$

The quantities $\omega_r{}^V$ defined in Eq. (A.4) and $\omega_r{}^W$ which can be similarly derived are the lateral in plane and out of plane natural frequencies of the ropes at the car side. The coefficients $\zeta_r{}^V$ and $\zeta_r{}^W$ represent the modal damping ratios in the lateral in plane and out of plane direction for the ropes at the car side. The coefficients $k_{rn}{}^{V1}$ defined in Eq. (A.5) and $k_{rn}{}^{W1}$ which can be obtained correspondingly, are the lateral in plane and out of plane linear stiffness coefficients of the ropes at the car side. In the stiffness coefficients of $k_{rn}{}^{V1}$ and $k_{rn}{}^{W1}$ are located the parametric terms which are the kinematic forcing terms that are exciting the ropes at the machine room level in the lateral in plane and out of plane direction resulting in a parametric excitation to the ropes. The coefficients $k_{rn}{}^{V2}$ defined in Eq. (A.6) and $k_{rn}{}^{W2}$ which can be similarly derived are the lateral parameters that account for the linear coupling terms between the lateral in plane and out of plane displacements for the ropes at the car side. The coefficients $k_{rn}{}^{V3}$ and $k_{rn}{}^{V4}$ defined in Eqs. (A.7) and (A.8) represents the lateral in plane parameters that account for the linear coupling terms with the longitudinal modal displacements of the elevator car and compensating sheave for the ropes at the car side. The coefficients $k_{rn}{}^{W3}$ and $k_{rn}{}^{W4}$ represents the lateral out of plane parameters that account for the linear coupling terms with the longitudinal modal displacements of the elevator car and compensating sheave for the ropes at the car side.

The coefficients $D_{rn}{}^{V1}$, $D_{rn}{}^{V2}$, $D_{rn}{}^{V3}$, $R_{rnjp}{}^{V1}$, $R_{rnjp}{}^{V2}$ defined in Eqs. (A.9)–(A.11), and (A.14) account for the lateral quadratic and cubic nonlinear terms in the lateral in plane direction of the ropes at the car side. The coefficients $D_{rn}{}^{V4}$, $D_{rn}{}^{V5}$ defined in Eqs. (A.12), (A.13) and $D_{rn}{}^{W4}$, $D_{rn}{}^{W5}$ which can be derived similarly account for the lateral quadratic terms, coupling between the longitudinal modes of the elevator car and compensating sheave and the lateral in plane and out of plane directions of the ropes at the car side, due to which the autoparametric (2:1) resonance may occur. The coefficients $D_{rn}{}^{W1}$, $D_{rn}{}^{W2}$, $D_{rn}{}^{W3}$, $R_{rnjp}{}^{W1}$, and $R_{rnjp}{}^{W2}$ account for the lateral quadratic and cubic nonlinear terms in the lateral out of plane direction of the ropes at the car side.

According to Nayfeh and Mook [38], whirling motions of the rope is a nonlinear phenomenon which occur in systems that can be represented by nonlinear string models. The whirling motion of a rope occurs when the energy of the rope is transferred from the lateral in plane direction to the lateral out of plane direction. These motions are a direct consequence of the fact that the frequency of motion in the plane of the excitation is the same as the frequency of the motion in the plane perpendicular to the plane of the excitation. Thus, a 1:1 autoparametric internal resonance occur when the lateral in plane and out of plane natural frequencies of the ropes at the car side represented by $\omega_r{}^V$ and $\omega_r{}^W$ are equal and is due to the cubic nonlinear terms in Eqs. (69) and (70) from the coefficients $R_{rnjp}{}^{V2}$ and $R_{rnjp}{}^{W1}$ where the coupling between the lateral in plane and out of plane modes occur.

The coefficients $F_r{}^V$ defined in Eq. (A.15) and $F_r{}^W$ which can be derived similarly are the excitation forces in the lateral in plane and out of plane direction of the ropes at the car side.

The equations of motion for the counterweight side for $i = 3,4$ are the following:

$$\begin{aligned}
&\ddot{q}_{ir}(t) + 2\zeta_{ir}^V \omega_r^{V(i)} \dot{q}_{ir}(t) + \left(\omega_r^{V(i)}\right)^2 q_{ir}(t) + \sum_{n=1}^{N} k_{irn}^V q_{in}(t) \\
&\quad + \sum_{n=1}^{N}\left(D_{irn}^{V1} U_{CS} + D_{irn}^{V2} U_{CW}\right) q_{in}(t) \\
&+ \sum_{n=1}^{N}\sum_{j=1}^{N}\sum_{p=1}^{N} R_{irnjp}^{V1} q_{ij}^2(t) q_{in}(t) + \sum_{n=1}^{N}\sum_{j=1}^{N}\sum_{p=1}^{N} R_{irnjp}^{V2} c_{ij}^2(t) q_{in}(t) + F_{ir}^V = 0
\end{aligned} \tag{71}$$

$$\begin{aligned}
&\ddot{c}_{ir}(t) + 2\zeta_{ir}^W \omega_r^{W(i)} \dot{c}_{ir}(t) + \left(\omega_r^{W(i)}\right)^2 c_{ir}(t) + \sum_{n=1}^{N} k_{irn}^W c_{in}(t) \\
&\quad + \sum_{n=1}^{N}\left(D_{irn}^{W1} U_{CS} + D_{irn}^{W2} U_{CW}\right) c_{in}(t) \\
&+ \sum_{n=1}^{N}\sum_{j=1}^{N}\sum_{p=1}^{N} R_{irnjp}^{W1} q_{ij}^2(t) c_{in}(t) + \sum_{n=1}^{N}\sum_{j=1}^{N}\sum_{p=1}^{N} R_{irnjp}^{W2} c_{ij}^2(t) c_{in}(t) + F_{ir}^W = 0
\end{aligned} \tag{72}$$

The quantities $\omega_r{}^{V(i)}$ defined in Eqs. (A.17) and (A.24), and the quantities $\omega_r{}^{W(i)}$ which can be derived similarly are the lateral in plane and out of plane natural frequencies for the ith rope at the counterweight side. The coefficients $\zeta_{ir}{}^V$ and $\zeta_{ir}{}^W$ represent the modal damping ratios for the ith rope in the lateral in plane and out of plane direction. The coefficients $k_{irn}{}^V$ defined in Eqs. (A.18) and (A.25), and the coefficients $k_{irn}{}^W$ which can be obtained similarly are the lateral in plane and out of plane linear stiffness coefficients for the ropes at the counterweight side. In the stiffness coefficients of $k_{irn}{}^V$ and $k_{irn}{}^W$ are located the parametric terms which are the kinematic forcing terms that are exciting the ropes at the machine room level in the lateral in plane and out of plane direction resulting in a parametric excitation to the ropes. The coefficients $R_{irnjp}{}^{V1}$ and $R_{irnjp}{}^{V2}$ defined in Eqs. (A.21) and (A.28) account for the lateral cubic nonlinear terms in the lateral in plane direction of the ropes at the counterweight side. The coefficients $R_{irnjp}{}^{W1}$ and $R_{irnjp}{}^{W2}$ account for the lateral cubic nonlinear terms in the lateral out of plane direction of the ropes at the counterweight side. The coefficient $D_{irn}{}^{V1}$ and $D_{irn}{}^{V2}$ defined in Eqs. (A.19), (A.20), (A.26), and (A.27), and $D_{irn}{}^{W1}$ and $D_{irn}{}^{W2}$ which can be derived correspondingly account for the lateral quadratic terms coupling between the longitudinal modes of the compensating sheave and counterweight and the lateral in plane and out of plane direction of the ropes at the counterweight side, due to which the autoparametric (2:1) resonance may occur. The autoparametric (1:1) internal resonance takes place between the lateral in plane and out of plane directions represented by $\omega_r{}^{V(i)}$ and $\omega_r{}^{W(i)}$ are equal and is due to the cubic nonlinear terms of Eqs. (71) and (72) from the coefficients

$R_{irnjp}{}^{V2}$ and $R_{irnjp}{}^{W1}$ where the coupling between the lateral in plane and out of plane modes occur.

The coefficients $F_{ir}{}^{V}$ defined in Eqs. (A.22) and (A.29) and $F_{ir}{}^{W}$ which can be derived correspondingly are the excitation forces in the lateral in plane and out of plane direction of the ropes at the counterweight side. All of the coefficients are coming from solving the integrals from the Galerkin Method.

The equations of motion for the elevator car, compensating sheave and counterweight are shown in the following equations:

$$\begin{aligned} &M_1\left(U_{CR}\right)_{tt} + k^{u1}U_{CR}(t) + k^{u2}U_{CS}(t) + \sum_{n=1}^{N} k_n^{u3}q_n(t) + \sum_{n=1}^{N} k_n^{u4}c_n(t) \\ &\quad + \sum_{j=1}^{N}\sum_{p=1}^{N} R_{jp}^{u1}q_j(t)q_p(t) \\ &+ \sum_{j=1}^{N}\sum_{p=1}^{N} R_{jp}^{u2}c_j(t)c_p(t) + f_{CR} = 0 \end{aligned}, \tag{73}$$

$$\begin{aligned} &M_2\left(U_{CS}\right)_{tt} + \bar{k}^{u1}U_{CR}(t) + \bar{k}^{u2}U_{CS}(t) + \bar{k}^{u3}U_{CW}(t) \\ &\quad + \sum_{n=1}^{N} \bar{k}_n^{u4}q_n(t) + \sum_{n=1}^{N} \bar{k}_n^{u5}c_n(t) \\ &+ \sum_{j=1}^{N}\sum_{p=1}^{N} \bar{R}_{jp}^{u1}q_j(t)q_p(t) + \sum_{j=1}^{N}\sum_{p=1}^{N} \bar{R}_{jp}^{u2}c_j(t)c_p(t) + \sum_{n=1}^{N} \bar{R}_n^{u3}q_{3n}^2(t), \\ &\quad + \sum_{n=1}^{N} \bar{R}_n^{u4}c_{3n}^2(t) + f_{CS} = 0 \end{aligned} \tag{74}$$

$$\begin{aligned} &M_3\left(U_{CW}\right)_{tt} + \hat{k}^{u1}U_{CS}(t) + \hat{k}^{u2}U_{CW}(t) + \sum_{n=1}^{N} \hat{R}_n^{u1}q_{3n}^2(t) \\ &\quad + \sum_{n=1}^{N} \hat{R}_n^{u2}c_{3n}^2(t) + \sum_{n=1}^{N} \hat{R}_n^{u3}q_{4n}^2(t) \\ &+ \sum_{n=1}^{N} \hat{R}_n^{u4}c_{4n}^2(t) + f_{CW} = 0 \end{aligned}. \tag{75}$$

The coefficients k^{u1}, $\bar{k}^{u2}$, and $\hat{k}^{u2}$ defined in Eqs. (A.30), (A.37), and (A.45) are the longitudinal linear stiffness parameters. The coefficients k^{u2}, $\bar{k}^{u1}$, $\bar{k}^{u3}$, and $\hat{k}^{u1}$ defined in Eqs. (A.31), (A.36), (A.38), and (A.44) are the longitudinal parameters that account for the linear coupling terms with the longitudinal displacements of the elevator car, compensating sheave, and counterweight. The coefficients $k_n{}^{u3}$ and $k_n{}^{u4}$ defined in Eqs. (A.32) and (A.33) are the lateral in plane and out of plane parameters that account for the linear coupling terms with the longitudinal displacements of the elevator car. The coefficients $\bar{k}_n{}^{u4}$ and $\bar{k}_n{}^{u5}$ defined in Eqs. (A.39) and (A.40) are the lateral in plane and out of plane parameters that account for the linear coupling terms with the longitudinal displacements of the compensating sheave.

The coefficients R^{u1}, R^{u2}, $\bar{R}^{u1}$, $\bar{R}^{u2}$, $\bar{R}^{u3}$, $\bar{R}^{u4}$, $\hat{R}^{u1}$, $\hat{R}^{u2}$, $\hat{R}^{u3}$, and $\hat{R}^{u4}$ defined in Eqs. (A.34), (A.41), (A.42), (A.46), and (A.47) account for the lateral in plane and out of plane quadratic nonlinear terms in the longitudinal direction of the elevator car, compensating sheave, and counterweight.

The coefficients F_{CR}, F_{CS}, and F_{CW} defined in Eqs. (A.35), (A.43), and (A.48) are the excitation forces in the longitudinal direction of the elevator car, compensating sheave, and counterweight. All of the coefficients are coming from solving the integrals from the Galerkin Method.

The equations of motion (73)–(75) describe the longitudinal behaviour of the elevator car, compensating sheave, and counterweight, respectively, and can be transformed into the modal coordinates using the transformation $\vec{U} = [Y]\vec{S}$ where $\vec{U} = [U_{CR}\ U_{CS}\ U_{CW}]^T$ and $\vec{S} = [S_1\ S_2\ S_3]^T$ is a vector of modal-coordinates corresponding to the three longitudinal modes of the system, respectively. If $[Y]$ is the mass-normalized mode shape matrix, the following equation in a matrix form describes the vertical response of the car, compensating sheave and counterweight in terms of the modal parameters

$$\ddot{\vec{S}}(t) + [C]\dot{\vec{S}}(t) + [P]\vec{S}(t) + [Y]^T\left(\vec{\sigma}_1 + \vec{\sigma}_2\right) + [Y]^T\left(\vec{F} + \vec{\eta}\right) = 0, \tag{76}$$

where the matrices *[C]* and *[P]* are defined by (77) and (78), respectively.

$$[C] = \begin{bmatrix} 2\zeta_1\omega_1 & 0 & 0 \\ 0 & 2\zeta_2\omega_2 & 0 \\ 0 & 0 & 2\zeta_3\omega_3 \end{bmatrix}. \tag{77}$$

$$[P] = \begin{bmatrix} \omega_1^2 & 0 & 0 \\ 0 & \omega_2^2 & 0 \\ 0 & 0 & \omega_3^2 \end{bmatrix}. \tag{78}$$

The quantities ω_1, ω_2, and ω_3 represent the longitudinal natural frequencies of the system. The longitudinal natural frequencies can be estimated by obtaining the eigenvalues with the characteristic equation defined by (79), where λ represent the eigenvalues of the stiffness matrix K_M defined in (80) and I represent the identity matrix. The coefficients ζ_1, ζ_2, ζ_3 represent the three longitudinal modal damping ratios of the system. The vectors $\vec{\sigma}_1$, $\vec{\sigma}_2$, $\vec{F}$, $\vec{\eta}$ are shown in Eqs. (81)–(84).

$$\det\left(K_M - \lambda I\right) = 0, \tag{79}$$

$$K_M = \begin{bmatrix} \frac{k^{u1}}{M_1} & \frac{k^{u2}}{M_1} & 0 \\ \frac{\bar{k}^{u1}}{M_2} & \frac{\bar{k}^{u2}}{M_2} & \frac{\bar{k}^{u3}}{M_2} \\ 0 & \frac{\hat{k}^{u1}}{M_3} & \frac{\hat{k}^{u2}}{M_3} \end{bmatrix}, \tag{80}$$

$$\vec{\sigma}_1 = \begin{bmatrix} \sum_{n=1}^{N} k_n^{u3}q_n(t) \\ \sum_{n=1}^{N} \bar{k}_n^{u4}q_n(t) \\ 0 \end{bmatrix}, \tag{81}$$

$$\vec{\sigma}_2 = \begin{bmatrix} \sum_{n=1}^{N} k_n^{u4}c_n(t) \\ \sum_{n=1}^{N} \bar{k}_n^{u5}c_n(t) \\ 0 \end{bmatrix}, \tag{82}$$

$$\vec{F} = \begin{bmatrix} f_{CR} \\ f_{CS} \\ f_{CW} \end{bmatrix}, \tag{83}$$

$$\vec{\eta} = \begin{bmatrix} \eta_{CR} \\ \eta_{CS} \\ \eta_{CW} \end{bmatrix}, \tag{84}$$

The coefficients η_{CR}, η_{CS}, η_{CW} represent the quadratic terms that feature in the equations of motion of the elevator car, compensating sheave, counterweight represented by the following equations:

$$\eta_{CR} = \sum_{j=1}^{N}\sum_{p=1}^{N} R_{jp}^{u1}q_j(t)q_p(t) + \sum_{j=1}^{N}\sum_{p=1}^{N} R_{jp}^{u2}c_j(t)c_p(t), \tag{85}$$

$$\begin{aligned} \eta_{CS} &= \sum_{j=1}^{N}\sum_{p=1}^{N} \bar{R}_{jp}^{u1}q_j(t)q_p(t) + \sum_{j=1}^{N}\sum_{p=1}^{N} \bar{R}_{jp}^{u2}c_j(t)c_p(t) \\ &\quad + \sum_{n=1}^{N} \bar{R}_n^{u3}q_{3n}^2(t) + \sum_{n=1}^{N} \bar{R}_n^{u4}c_{3n}^2(t), \end{aligned} \tag{86}$$

$$\eta_{CW} = \sum_{n=1}^{N} \hat{R}_n^{u1}q_{3n}^2(t) + \sum_{n=1}^{N} \hat{R}_n^{u2}c_{3n}^2(t) + \sum_{n=1}^{N} \hat{R}_n^{u3}q_{4n}^2(t) + \sum_{n=1}^{N} \hat{R}_n^{u4}c_{4n}^2(t). \tag{87}$$

Similarly in Eqs. (69)–(72) the coefficients of the elevator car, compensating sheave and counterweight are transformed and rewritten as

the following equations

$$\ddot{q}_r(t) + 2\zeta_r^V \omega_r^V \dot{q}_r(t) + \left(\omega_r^V\right)^2 q_r(t) + \sum_{n=1}^{N} k_{rn}^{V1} q_n(t) + \bar{\sigma}_u^V \vec{Y}^{(1)} S_1 + \bar{\sigma}_u^V \vec{Y}^{(2)} S_2 + \bar{\sigma}_u^V \vec{Y}^{(3)} S_3 + \sum_{n=1}^{N} k_{rn}^{V2} c_n(t) + \sum_{n=1}^{N}\sum_{j=1}^{N} D_{rn}^{V1} q_j(t) q_n(t) + \sum_{n=1}^{N}\sum_{j=1}^{N} D_{rn}^{V2} c_j(t) q_n(t) + \sum_{n=1}^{N}\sum_{j=1}^{N} D_{rn}^{V3} c_j(t) c_n(t) + \sum_{n=1}^{N}\left(D_{rn}^{V4}\vec{Y}^{(1)}\vec{S} + D_{rn}^{V5}\vec{Y}^{(2)}\vec{S}\right) q_n(t) + \sum_{n=1}^{N}\sum_{j=1}^{N}\sum_{p=1}^{N} R_{rnjp}^{V1} q_j(t) q_p(t) q_n(t) + \sum_{n=1}^{N}\sum_{j=1}^{N}\sum_{p=1}^{N} R_{rnjp}^{V2} c_j(t) c_p(t) q_n(t) + F_r^V = 0 \quad (88)$$

$$\ddot{c}_r(t) + 2\zeta_r^W \omega_r^W \dot{c}_r(t) + \left(\omega_r^W\right)^2 c_r(t) + \sum_{n=1}^{N} k_{rn}^{W1} c_n(t) + \bar{\sigma}_u^W \vec{Y}^{(1)} S_1 + \bar{\sigma}_u^W \vec{Y}^{(2)} S_2 + \bar{\sigma}_u^W \vec{Y}^{(3)} S_3 + \sum_{n=1}^{N} k_{rn}^{W2} q_n(t) + \sum_{n=1}^{N}\sum_{j=1}^{N} D_{rn}^{W1} q_j(t) c_n(t) + \sum_{n=1}^{N}\sum_{j=1}^{N} D_{rn}^{W2} c_j(t) c_n(t) + \sum_{n=1}^{N}\sum_{j=1}^{N} D_{rn}^{W3} q_j(t) q_n(t) + \sum_{n=1}^{N}\left(D_{rn}^{W4}\vec{Y}^{(1)}\vec{S} + D_{rn}^{W5}\vec{Y}^{(2)}\vec{S}\right) c_n(t) + \sum_{n=1}^{N}\sum_{j=1}^{N}\sum_{p=1}^{N} R_{rnjp}^{W1} q_j(t) q_p(t) c_n(t) + \sum_{n=1}^{N}\sum_{j=1}^{N}\sum_{p=1}^{N} R_{rnjp}^{W2} c_j(t) c_p(t) c_n(t) + F_r^W = 0 \quad (89)$$

$$\ddot{q}_{ir}(t) + 2\zeta_{ir}^V \omega_r^{V(i)} \dot{q}_{ir}(t) + \left(\omega_r^{V(i)}\right)^2 q_{ir}(t) + \sum_{n=1}^{N} k_{irn}^V q_{in}(t) + \sum_{n=1}^{N}\left(D_{irn}^{V1}\vec{Y}^{(2)}\vec{S} + D_{irn}^{V2}\vec{Y}^{(3)}\vec{S}\right) q_{in}(t) + \sum_{n=1}^{N}\sum_{j=1}^{N}\sum_{p=1}^{N} R_{irnjp}^{V1} q_{ij}^2(t) q_{in}(t) + \sum_{n=1}^{N}\sum_{j=1}^{N}\sum_{p=1}^{N} R_{irnjp}^{V2} c_{ij}^2(t) q_{in}(t) + F_{ir}^V = 0 \quad (90)$$

$$\ddot{c}_{ir}(t) + 2\zeta_{ir}^W \omega_r^{W(i)} \dot{c}_{ir}(t) + \left(\omega_r^{W(i)}\right)^2 c_{ir}(t) + \sum_{n=1}^{N} k_{irn}^W c_{in}(t) + \sum_{n=1}^{N}\left(D_{irn}^{W1}\vec{Y}^{(2)}\vec{S} + D_{irn}^{W2}\vec{Y}^{(3)}\vec{S}\right) c_{in}(t) + \sum_{n=1}^{N}\sum_{j=1}^{N}\sum_{p=1}^{N} R_{irnjp}^{W1} q_{ij}^2(t) c_{in}(t) + \sum_{n=1}^{N}\sum_{j=1}^{N}\sum_{p=1}^{N} R_{irnjp}^{W2} c_{ij}^2(t) c_{in}(t) + F_{ir}^W = 0 \quad (91)$$

where $\bar{\sigma}_u{}^V$ and $\bar{\sigma}_u{}^W$ represented by:

$$\bar{\sigma}_u^V = \begin{bmatrix} k_r^{V3} & k_r^{V4} & 0 \end{bmatrix}, \quad (92)$$

$$\bar{\sigma}_u^W = \begin{bmatrix} k_r^{W3} & k_r^{W4} & 0 \end{bmatrix}. \quad (93)$$

3. Case study and simulation

A summary of the parameters used in the simulation tests are shown in Table 1.

The analysis is focused on the car side subsystem. In this simulation the longitudinal natural frequency of the car corresponding to the position of the car along the travel height of ω_1 is chosen to be twice the lateral in plane natural frequency of the suspension ropes at the car side ($\omega_1 = 2\omega_1{}^V$) and the external excitation frequency in the lateral in plane direction of the building structure should coincide with the lateral in plane natural frequency of the suspension ropes at the car side $\Omega_V = \omega_1{}^V$.

The research to analyse wind loading acting on a building structure has attracted the attention of many researchers. For example in [40,41] the formation of vortices, distortion of the mean flow, and flow separation has been considered. Large aerodynamic loads act on the building structure which makes the building vibrate in rectilinear and torsional modes, as discussed in [41]. Full scale monitoring was carried out in [42] to better understand the methodology used to predict the acceleration response of high-rise buildings consistent with on-site behaviour. A full scale monitoring programme has been discussed in [43,44]. The results presented corresponded to the first three natural frequencies, modal damping ratios and mode shapes for three building structures. A comparison is then developed between the measurement data, simulation results from finite element models and wind tunnel testing. Thus, following the results presented in [43,44], the frequency of excitation in the lateral in plane and in the lateral out of plane directions for the simulation tests is assumed to be harmonic and corresponds to the fundamental modes of the structure, relevant parameters are shown in Table 1.

The stiffness coefficients of the springs that are connected to the elevator car in the lateral in plane direction and in the lateral out of plane direction can be calculated using Eqs. (1)–(3), resulting in $k_1 = 80$ kN/m and $k_2 = 236$ kN/m when using hard tyres and $k_1 = 30$ kN/m and $k_2 = 75$ kN/m when using soft tyres. Following on from what has been discussed in Section 2, the total combined stiffness of the system in the lateral in plane and out of plane direction depends on the stiffness of the elevator car suspension-tyre system when using hard or soft tyres. In the considerations to follow it is assumed that the lateral in plane and lateral out of plane natural frequencies of the elevator car, suspension, and compensating ropes system at the car side are the same ($\omega_1{}^V \approx \omega_1{}^W$). The stiffness coefficients of the springs in the lateral in plane and out of plane direction are assumed to be equal, and are taken as $k_1 = k_2 = 80$ kN/m when using hard tyres and $k_1 = k_2 = 30$ kN/m when using soft tyres, respectively. The simulation tests cover the time interval of 200 s.

3.1. Frequency analysis

The variation of frequency corresponding to all lateral modes of the elevator car, suspension, and compensating ropes at the car side according to the position of the elevator car in the hoistway measured from the bottom landing level are shown in Fig. 4, with $k_1 = k_2 = 80$ kN/m.

In Fig. 4 the solid blue, green, magenta, and cyan lines represent the variation of frequency of the first four lateral natural frequencies at the car side lateral subsystem, which is composed of the elevator car mass, the suspension and compensating ropes. The variation of the lateral in plane and out of plane natural frequencies at the car side of the elevator car, suspension and compensating ropes are the same as shown in Fig. 4, due to $k_1 = k_2$ according to the initial input data presented at the beginning of this chapter. The dashed green line represents the variation of frequency of the first longitudinal natural frequency in the vertical direction. The dashed magenta and black lines represent the fundamental natural frequency of the suspension and compensating ropes, respectively, when the interface between the car and the hoistway is considered as rigid and the car mass lateral motions are not admitted. The horizontal dashed red and blue lines represent the excitation frequencies of the building structure in the lateral in plane and out of plane direction with 0.42 Hz and 0.36 Hz, respectively.

It is evident from Fig. 4 that the suspension ropes will be excited at the fundamental natural frequency when the car is positioned at 72.0 m from the bottom landing level in the lateral out of plane direction due to the frequency of excitation of the building structure in the lateral out of plane direction of 0.36 Hz. If the car is positioned at 120.0 m from the bottom landing level the compensating ropes will be excited at the fundamental natural frequency.

When the elevator car is at a height of approximately 100.0 m the first natural frequency in the longitudinal direction is twice the fundamental natural frequency of the elevator car, suspension, and compensating ropes at the car side. For the condition $\Omega_V \approx \omega_1/2 \approx \omega_1{}^{V/W}$, the external excitation of the building structure in the lateral in plane direction was set at the fundamental natural frequency of the elevator car, suspension and compensating ropes at the car side in the lateral in plane and out of plane direction when the car is positioned at the height of 100.0 m.

In Fig. 4 the curve veering phenomena is observed which is when two eigenvalues approach each other closely and suddenly veer away again,

Table 1
Summary of parameters used in the simulation tests.

System parameters	
Number of suspension ropes	$n_1 = 6$
Number of compensating ropes	$n_2 = 6$
Mass per unit length of suspension ropes	$m_1 = 2.15$ kg/m
Mass per unit length of compensating ropes	$m_2 = 2.15$ kg/m
Elastic modulus of suspension ropes	$EA_1 = 95{,}276{,}193$ N
Elastic modulus of compensating ropes	$EA_2 = 95{,}276{,}193$ N
Height	$h_0 = 248.0$ m
Travel height	$h_{trav} = 236.00$ m
Car mass with full load	$M_1 = 8600$ kg
Mass of the compensating sheave	$M_2 = 21{,}500$ kg
Mass of the counterweight	$M_3 = 7800$ kg
Height measured from the bottom landing level to the centre of the compensating sheave	$b_1 = 8.30$ m
Height from centre of the traction sheave to the centre of the diverter pulley	$b_2 = 0.50$ m
Frequency of excitation in the lateral in plane direction	$\Omega_V = 2.64$ rad/s (0.42 Hz)
Frequency of excitation in the lateral out of plane direction	$\Omega_W = 2.26$ rad/s (0.36 Hz)
Displacement at the machine room level in the lateral in plane direction	$A_V = 0.15$ m
Displacement at the machine room level in the lateral out of plane direction	$A_W = 0.15$ m
Young's modulus of elasticity of the guide rail	$E_G = 210 \times 10^9$ N/m^2
T cross section flange width	$a_1 = 60$ mm
T cross section web height	$a_2 = 70$ mm
T cross section thickness	$a_3 = 6$ mm
2nd moment of inertia of the T cross-sectional area in the lateral in plane direction	$J_y = 2.87 \times 10^{-7}$ m^4
2nd moment of inertia of the T cross-sectional area in the lateral out of plane direction	$J_z = 9.20 \times 10^{-7}$ m^4
Length of the guide rail section	$L_G = 5.00$ m
Stiffness of the elevator car suspension-tyre with hard tyres [30]	$K_c = 580$ kN/m
Stiffness of the elevator car suspension-tyre with soft tyres [39]	$K_c = 50$ kN/m

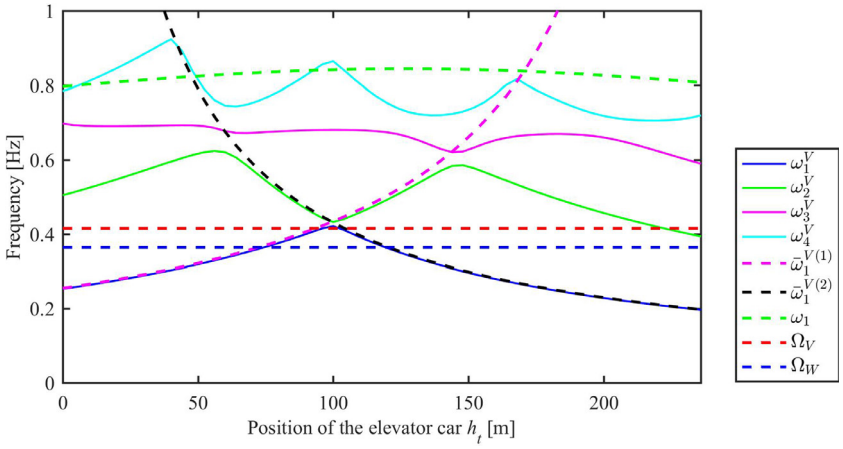

Fig. 4. Variation of the first four lateral natural frequencies at car side lateral subsystem ($\omega^V{}_{1/2/3/4}$) for $k_{1/2} = 80$ kN/m, $\bar{\omega}_1{}^{V(1/2)}$ – first lateral natural frequency of suspension and compensating ropes, ω_1 – first longitudinal natural frequency and $\Omega_{V/W}$ – excitation frequencies of building structure in lateral in plane and out of plane direction. (For interpretation of the references to colour in this figure legend, the reader is referred to the web version of this article.)

each one taking on the trajectory of the other, according to Giannini and Sestieri [45]. The veering phenomena is defined as smooth change of normal parametric variation of two modes approaching each other but, instead of crossing, they veer away and finally diverge [24,46–48].

In Fig. 5 the solid blue and green lines represent the variation of frequency of the first two lateral natural frequencies of the car side lateral subsystem vs. the car position in the shaft for $k_1 = k_2 = 80$ kN/m and the magenta and cyan lines represent the variation of frequency of the first two lateral natural frequencies at the car side lateral subsystem for $k_1 = k_2 = 30$ kN/m. The horizontal dashed red and blue lines represent the excitation frequencies of the building structure in the lateral in plane and out of plane direction with 0.42 Hz and 0.36 Hz, respectively. As shown in Fig. 5 if the stiffness parameter is lowered the variation of frequency becomes smoother and the sharp peak for the fundamental natural frequency is reduced from 0.42 Hz to about 0.36 Hz. The frequency of excitation of the building structure in the lateral out of plane direction of 0.36 Hz and the fundamental natural frequency of the car subsystem for $k_1 = k_2 = 30$ kN/m are equal when the elevator car is at a height approximately of 100.0 m.

Similarly, the variation of the natural frequencies of the compensating ropes at the counterweight side and the variation of the first three longitudinal natural frequencies according to the position of the car in the hoistway measured from the bottom landing level are shown in Fig. 6. The solid blue, green, magenta, and cyan lines represent the first four lateral natural frequencies of the compensating ropes. The dashed black, magenta, and green lines represent the three longitudinal natural frequencies of the system according to the position of the elevator car, estimated by finding the eigenvalues. The horizontal dashed red and blue lines represent the frequency of excitation from the building structure at 0.42 Hz and 0.36 Hz in the lateral in plane and out of plane direction. In the scenario considered in this case study the compensating rope at the counterweight side will be excited at close to the fundamental natural frequency in the lateral out of plane direction due to the frequency of excitation of the building structure when the car is position at 116.0 m from the bottom landing level.

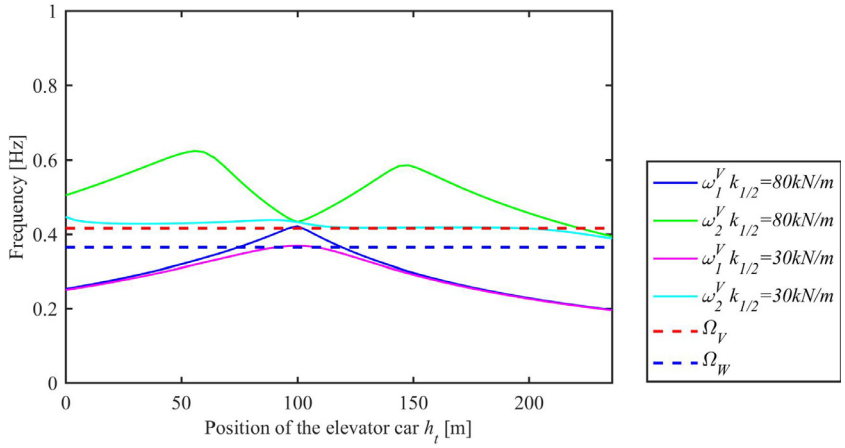

Fig. 5. Variation of the first two natural frequencies at car side lateral subsystem ($\omega^V{}_{1/2}$) for $k_{1/2}=80$ kN/m and $k_{1/2}=30$ kN/m, $\Omega_{V/W}$ – excitation frequencies of the building structure in the lateral in plane and out of plane direction. (For interpretation of the references to colour in this figure legend, the reader is referred to the web version of this article.)

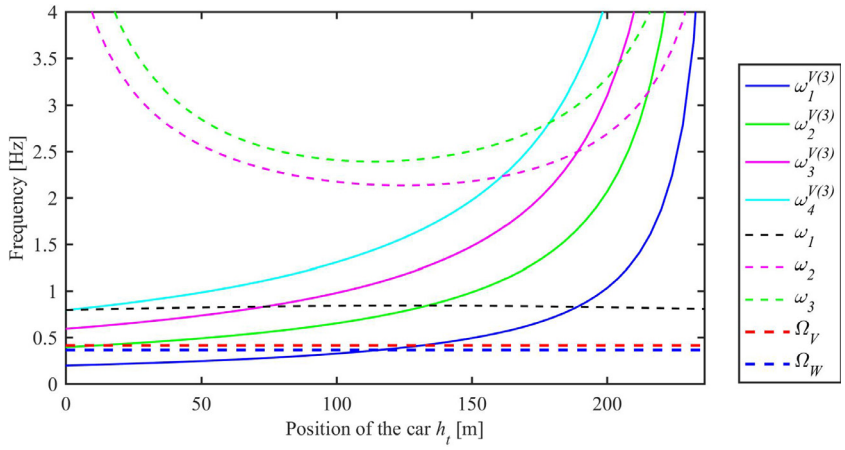

Fig. 6. Variation of the first four lateral natural frequencies of the compensating ropes at the counterweight side ($\omega^{V(3)}{}_{1/2/3/4}$), $\omega_{1/2/3}$ – first three longitudinal natural frequencies and $\Omega_{V/W}$ – the excitation frequencies of the building structure in the lateral in plane and out of plane direction. (For interpretation of the references to colour in this figure legend, the reader is referred to the web version of this article.)

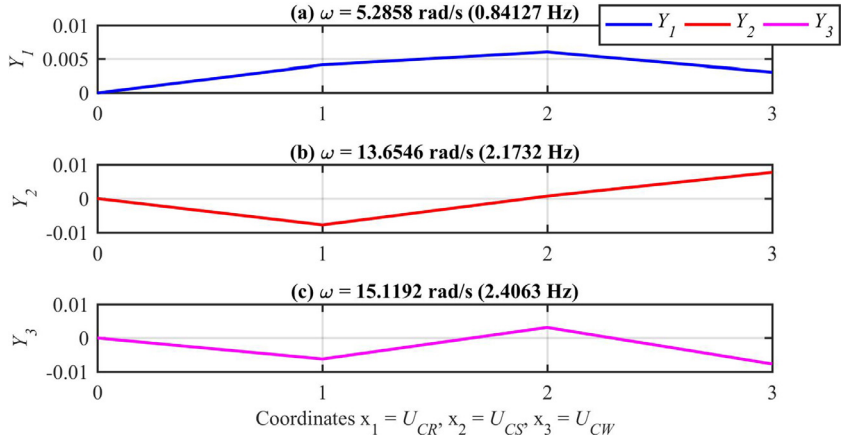

Fig. 7. The first three vertical mode shapes $Y_{1/2/3}$ of the elevator system.

3.2. Mode shapes

The mode shapes corresponding to the vertical vibrations of the elevator car, compensating sheave, and counterweight are shown in Fig. 7. In the first mode (0.84 Hz) the elevator car, compensating sheave, and counterweight are in phase. The second mode (2.17 Hz) the compensating sheave and counterweight are in phase than the elevator car. In the third mode (2.41 Hz) the elevator car and counterweight are in phase than the compensating sheave.

The 1st and 2nd lateral mode shapes at the car side subsystem composed of the suspension ropes, compensating ropes, and the elevator car when the car is at 100.0 m from the bottom landing level are shown in Fig. 8 and Fig. 9, respectively, comparing a $k_1=k_2=80$ kN/m and $k_1=k_2=30$ kN/m.

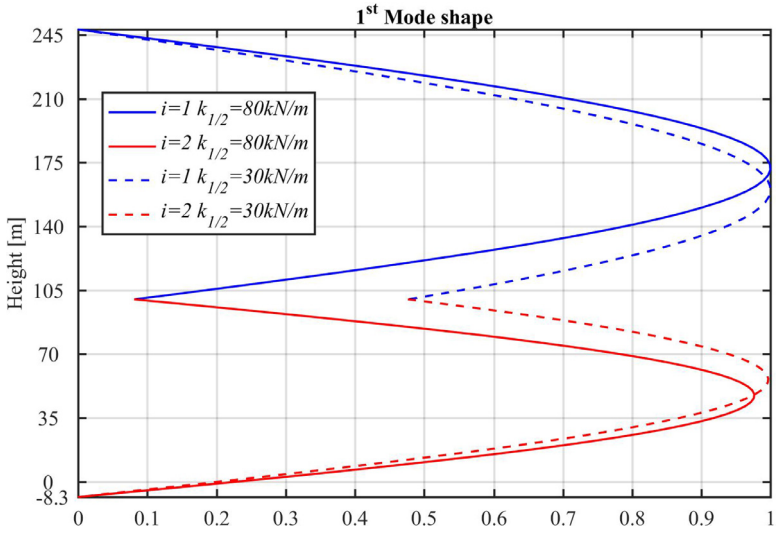

Fig. 8. First mode shapes of the system at the car side for $k_1 = k_2 = 80$ kN/m represented as solid line and $k_1 = k_2 = 30$ kN/m represented as dashed line, the suspension and compensating ropes are represented as blue and red lines. (For interpretation of the references to colour in this figure legend, the reader is referred to the web version of this article.)

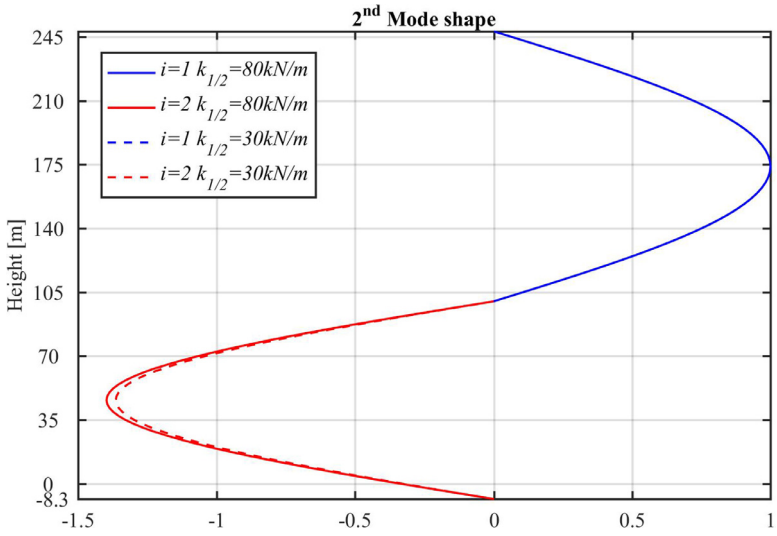

Fig. 9. Second mode shapes of the system at the car side for $k_1 = k_2 = 80$ kN/m represented as solid line and $k_1 = k_2 = 30$ kN/m represented as dashed line, the suspension and compensating ropes are represented as blue and red lines. (For interpretation of the references to colour in this figure legend, the reader is referred to the web version of this article.)

The solid line represents the mode shapes of the system at the car side subsystem when $k_1 = k_2 = 80$ kN/m and the dashed line represent the mode shapes of the system at the car side subsystem when $k_1 = k_2 = 30$ kN/m. The blue and red line correspond to the suspension ropes ($i = 1$) and compensating ropes ($i = 2$), respectively. The joining point where the blue and red lines meet represent the position of the elevator car considered as a lumped mass which is positioned at a height of 100.0 m from the bottom landing level. The bottom landing level is represented at 0.0 m. The height of −8.3 m is the height from the bottom landing level to the centre of the compensating sheave.

The sharp transition between the suspension and compensating ropes at the car subsystem for the 1st mode shape shown in Fig. 8 with a spring stiffness of $k_1 = k_2 = 80$ kN/m and $k_1 = k_2 = 30$ kN/m, is due to the fundamental mode shape of the ropes when the elevator car is positioned at a height of 100.0 m from the bottom landing level. It is evident from Fig. 8 that when using a low spring stiffness of $k_1 = k_2 = 30$ kN/m the lateral displacements of the elevator car are higher than using a high spring stiffness of $k_1 = k_2 = 80$ kN/m.

The 2nd mode shapes at the car side subsystem shown in Fig. 9 are the same when using a low spring stiffness $k_1 = k_2 = 30$ kN/m and a high spring stiffness $k_1 = k_2 = 80$ kN/m. The mode shapes are obtained with Eqs. (55) and (57). Similarly, the mode shapes at the counterweight side can be determined using Eq. (61).

3.3. Response of the ropes

The behaviour of all ropes are described by the mathematical model given in terms of Eqs. (88)–(91). The equations of motion are solved numerically by applying Runge–Kutta 4–5 order numerical algorithm to obtain the modal coordinates of the system. The total displacements of rope ith for $i = 1,2,3,4$ are obtain by using Eqs. (41)–(44) with the expansions of the system in the lateral in plane and out of plane directions defined in Eqs. (63) and (64).

The overall time response at the midspan length of the suspension and compensating ropes (defined by Eqs. (41) and (42)) at the car side when the elevator car is positioned at a height of 100.0 m from the bottom landing level are shown in Figs. 10 and 11.

The solution is for higher stiffness parameters of $k_1 = k_2 = 80$ kN/m represented by the blue line and for lower stiffness parameter of $k_1 = k_2 = 30$ kN/m represented by the red line. The response of the sus-

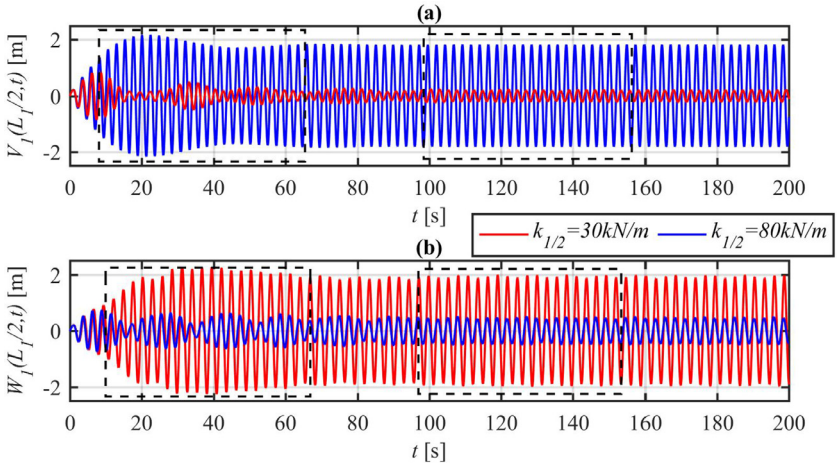

Fig. 10. The mid span length displacements of the suspension rope at the car side with respect to time (a) lateral in plane direction (b) lateral out of plane direction, $k_1 = k_2 = 80$ kN/m represented as blue line and $k_1 = k_2 = 30$ kN/m represented as red line, the elevator car is positioned at a height of 100.0 m from the bottom landing level. (For interpretation of the references to colour in this figure legend, the reader is referred to the web version of this article.)

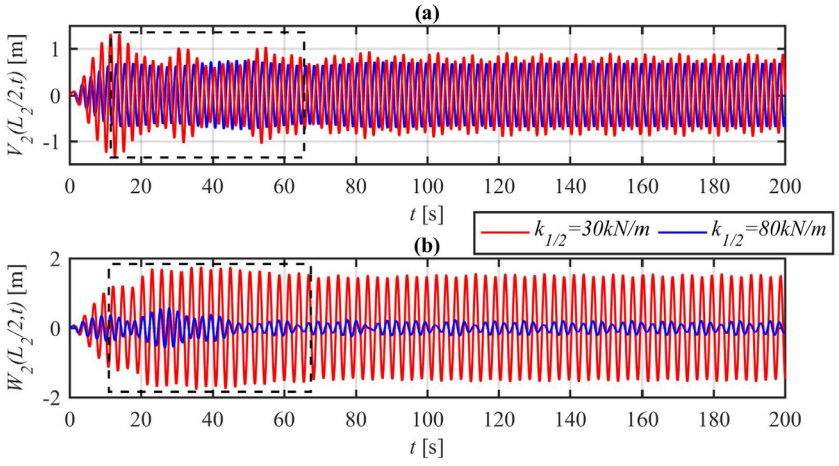

Fig. 11. The mid span length displacements of the compensating rope at the car side with respect to time (a) lateral in plane direction (b) lateral out of plane direction, $k_1 = k_2 = 80$ kN/m represented as blue line and $k_1 = k_2 = 30$ kN/m represented as red line, the elevator car is positioned at a height of 100.0 m from the bottom landing level. (For interpretation of the references to colour in this figure legend, the reader is referred to the web version of this article.)

pension and compensating ropes in the lateral in plane direction at the car side have high amplitudes at the start and during time the amplitudes decreases.

In Fig. 12(a) and (b) shows the maximum displacements of the compensating ropes at the car side in (a) lateral in plane and (b) lateral out of plane direction, with a high stiffness parameter of $k_1 = k_2 = 80$ kN/m represented by a dashed blue line and $k_1 = k_2 = 30$ kN/m represented by a dashed red line. The compensating rope length is measured from the centre of the compensating sheave to the elevator car considered as a lumped mass where the height is not considered. In Fig. 12(a) and (b) the shapes of the ropes display the first mode shape due to the excitation frequency of the building structure in the lateral in plane and out of plane directions.

The maximum displacements in the lateral in plane direction is 1.35 m and in the lateral out of plane direction is 1.82 m when the elevator car has a lower stiffness parameter of $k_1 = k_2 = 30$ kN/m. If the elevator shaft has a distance from wall to wall of 2.00 m in the lateral in plane and out of plane direction the ropes will impact the elevator shaft walls when the elevator car has a lower stiffness parameter of $k_1 = k_2 = 30$ kN/m.

The FFT frequency spectra of the lateral in plane and out of plane responses over the time span of 10.0 s–60.0 s for the suspension and compensating ropes at the car side are shown in Fig. 13(a)–(d) and Fig. 14(a)–(d), with a high stiffness parameter of $k_1 = k_2 = 80$ kN/m represented by a blue line and a low stiffness parameter of $k_1 = k_2 = 30$ kN/m represented by a red line.

The predominant frequencies are 0.42 Hz and 0.36 Hz which are the frequencies in which the building structure is exciting the ropes in the lateral in plane and out of plane directions. The frequency of 0.42 Hz in the lateral out of plane direction shown in Fig. 13(c) and Fig. 14(c) and the frequency of 0.36 Hz in the lateral in plane direction shown in Fig. 13(b) and Fig. 14(b) are the same external excitation frequency of the system in the lateral in plane and out of plane directions, respectively. Thus, 1:1 autoparametric interaction is taking place between the lateral in plane and out of plane directions, through the quadratic and cubic nonlinear terms of Eqs. (69) and (70) from the quadratic and cubic coefficients D_{rn}^{V2}, D_{rn}^{W1}, R_{rnjp}^{V2}, and R_{rnjp}^{W1} where the coupling between the lateral in plane and out of plane modes occur.

A third FFT frequency spectra is shown in Fig. 15(a) and (b) in the lateral in plane and (c) and (d) out of plane direction of the suspension ropes at the car side over a time span of 100.0 s–150.0 s, with a high stiffness parameter of $k_1 = k_2 = 80$ kN/m represented by a blue line and $k_1 = k_2 = 30$ kN/m represented by a red line. The maximum frequencies are 0.42 Hz shown in Fig. 15(a) and (b) in the lateral in plane direction and 0.36 Hz shown in Fig. 15(c) and (d) in the lateral out of plane di-

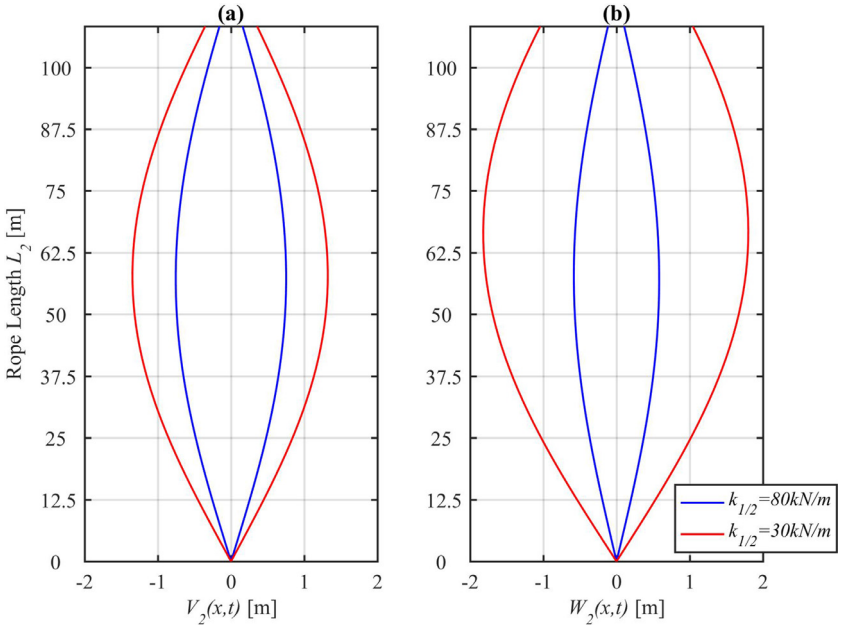

Fig. 12. The behaviour of the compensating ropes at the car side in (a) lateral in plane (b) lateral out of plane direction, $k_1 = k_2 = 80$ kN/m represented as blue line and $k_1 = k_2 = 30$ kN/m represented as red line. (For interpretation of the references to colour in this figure legend, the reader is referred to the web version of this article.)

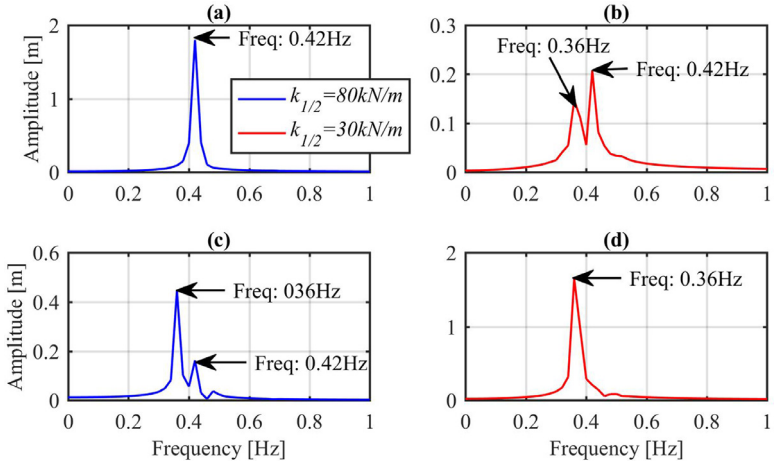

Fig. 13. FFT frequency spectra of suspension ropes at the car side (a) and (b) lateral in plane (c) and (d) lateral out of plane between a time span of 10.0 s–60.0 s, $k_1 = k_2 = 80$ kN/m represented as blue line and $k_1 = k_2 = 30$ kN/m represented as red line. (For interpretation of the references to colour in this figure legend, the reader is referred to the web version of this article.)

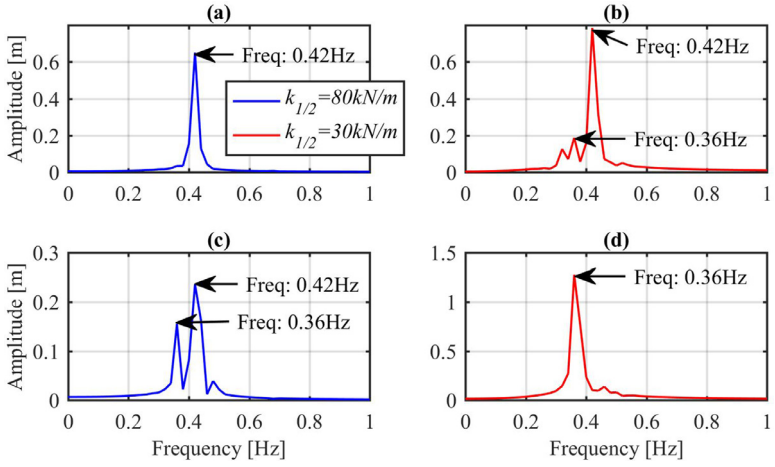

Fig. 14. FFT frequency spectra of compensating ropes at the car side (a) and (b) lateral in plane (c) and (d) lateral out of plane between a time span of 10.0 s–60.0 s, $k_1 = k_2 = 80$ kN/m represented as blue line and $k_1 = k_2 = 30$ kN/m represented as red line. (For interpretation of the references to colour in this figure legend, the reader is referred to the web version of this article.)

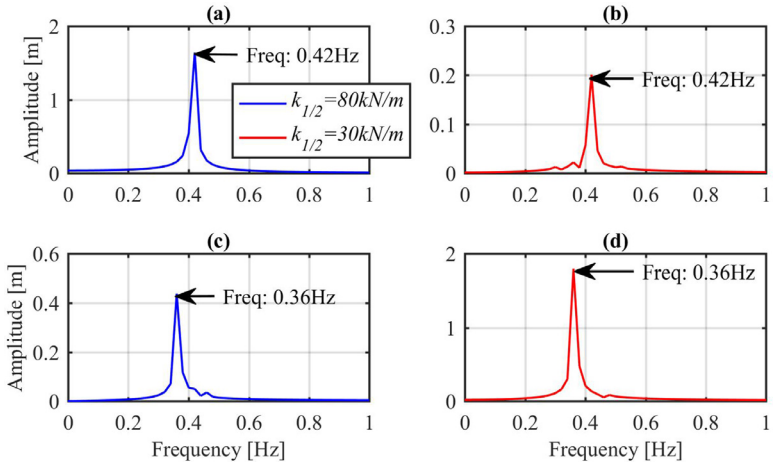

Fig. 15. FFT frequency spectra of suspension ropes at the car side (a) and (b) lateral in plane (c) and (d) lateral out of plane between a time span of 100.0 s–150.0 s, $k_1 = k_2 = 80$ kN/m represented as blue line and $k_1 = k_2 = 30$ kN/m represented as red line. (For interpretation of the references to colour in this figure legend, the reader is referred to the web version of this article.)

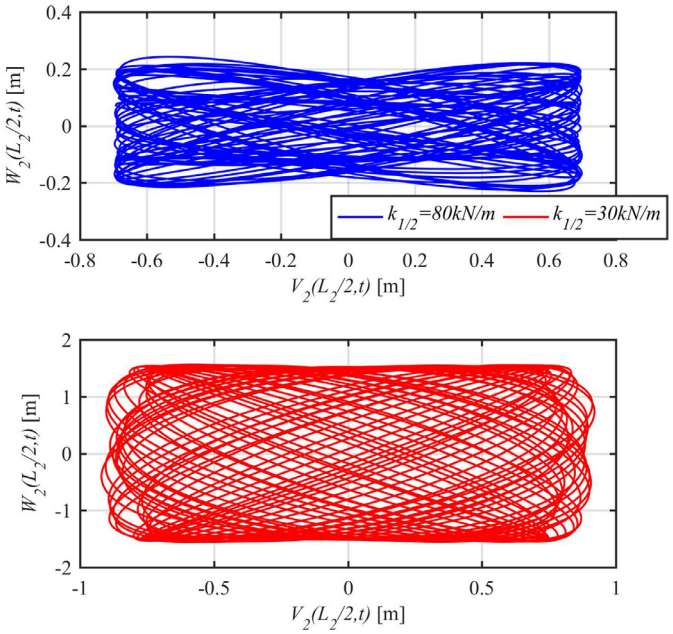

Fig. 16. Displacements of the compensating rope at the car side, $k_1 = k_2 = 80$ kN/m represented as blue line and $k_1 = k_2 = 30$ kN/m represented as red line, between 100.0 s and 200.0 s. (For interpretation of the references to colour in this figure legend, the reader is referred to the web version of this article.)

rection are the same as the external excitation applied to the system in the lateral in plane and out of plane direction.

The frequencies of 0.42 Hz and 0.36 Hz from the lateral in plane and out of plane directions are due to the parametric terms located in the lateral in plane and out of plane equations in the stiffness coefficients of $k_{rn}{}^{V1}$ and $k_{rn}{}^{W1}$. This parametric excitation is coming from the kinematic forcing terms that are exciting the ropes at the machine room level.

In Fig. 16(a) and (b) the motion of the compensating ropes at the car side can be observed between the time span of 100.0 s and 200.0 s when the displacements in the lateral in plane and out of plane direction are graphed together corresponding to the midspan length of the rope with a high stiffness parameter of $k_1 = k_2 = 80$ kN/m represented by a blue line shown in (a) and a low stiffness parameter of $k_1 = k_2 = 30$ kN/m represented by a red line shown in (b).

In Fig. 16(a) and (b) the full whirling motion of the compensating ropes at the car side subsystem is not developed due to the frequency of excitation of 0.36 Hz in the lateral out of plane direction is not equal to the frequency of excitation in the lateral in plane direction.

In order to develop the whirling motion of the suspension and compensating ropes at car side subsystem the frequency of excitation in the lateral in plane and out of plane direction should be approximately equal to the fundamental natural frequency of the suspension and compensating ropes at the car side subsystem ($\Omega_{V/W} \approx \omega_1{}^{V/W}$). The response of the compensating ropes at the car side subsystem shown in Fig. 17(a), (b) and Fig. 18 are obtained by assuming the external excitation frequency of the building structure in the lateral in plane and out of plane direction to be $\Omega_{V/W} = 2.64$ rad/s (0.42 Hz) with a high stiffness parameter of $k_1 = k_2 = 80$ kN/m and $\Omega_{V/W} = 2.26$ rad/s (0.36 Hz) with a low stiffness parameter of $k_1 = k_2 = 30$ kN/m. Assuming, the displacement at the machine room level in the lateral in plane direction is $A_V = 0.15$ m and in the lateral out of plane direction is $A_W = 0.02$ m. The other parameters considered at the beginning of Section 3 remain unchanged.

The overall time response at the midspan length of the compensating ropes at the car side when the elevator car is positioned at a height of 100.0 m from the bottom landing level is shown in Fig. 17(a) and (b). In Fig. 17(b) can be seen the displacements in the lateral out of plane direction increase over time due to the 1:1 autoparametric interaction is taking place between the lateral in plane and out of plane direction through the cubic nonlinear terms of Eqs. (69) and (70) where the coupling between the lateral in plane and out of plane modes occur. In Fig. 18 the motion of the compensating ropes at the car side can be observed between the time span of 100.0 s and 200.0 s when the displacements in the lateral in plane and out of plane direction are graphed together corresponding to the midspan length of the rope when the car is positioned at a height of 100.0 m from the bottom landing level with a high stiffness parameter of $k_1 = k_2 = 80$ kN/m represented by a blue line and a low stiffness parameter of $k_1 = k_2 = 30$ kN/m represented by a red line.

3.4. Lateral response of the elevator car

The lateral in plane and out of plane displacements of the elevator car relative to the building structure are shown in Fig. 19 with a high stiffness parameter of $k_1 = k_2 = 80$ kN/m represented by a blue line and in Fig. 20 with a low stiffness parameter of $k_1 = k_2 = 30$ kN/m represented by a red line in (a) and (b), respectively, compared with the displacements of the building structure represented by a dashed black line.

The maximum lateral in plane displacements of the elevator car relative to the building structure with a high stiffness parameter are 0.15 m

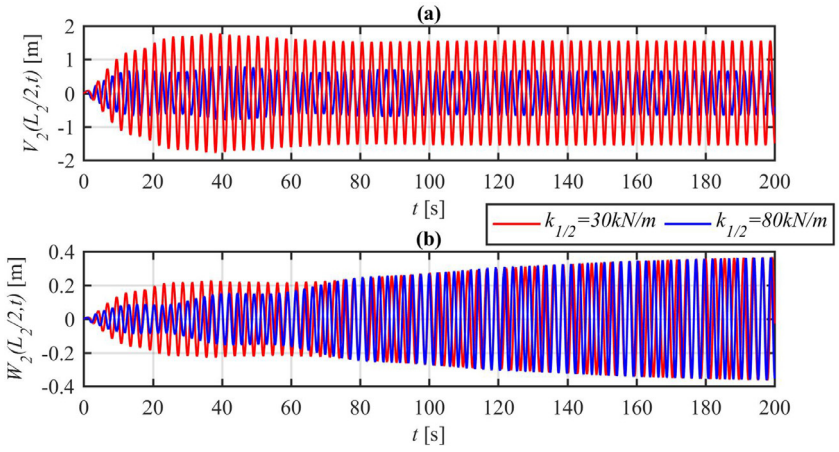

Fig. 17. The mid span length displacements of the compensating rope at the car side with respect to time (a) lateral in plane direction (b) lateral out of plane direction, $k_1 = k_2 = 80$ kN/m represented as blue line and $k_1 = k_2 = 30$ kN/m represented as red line, the elevator car is positioned at a height of 100.0 m from bottom landing level. (For interpretation of the references to colour in this figure legend, the reader is referred to the web version of this article.)

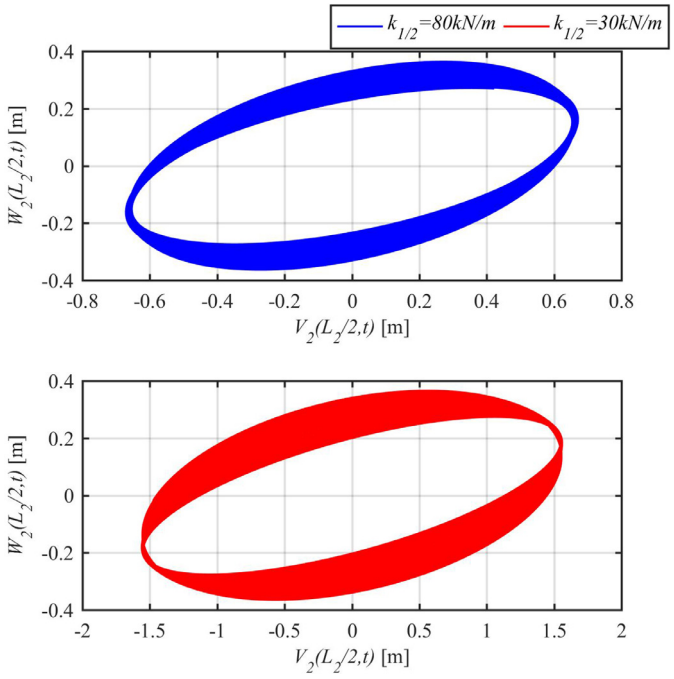

Fig. 18. Displacements of the compensating rope at the car side, $k_1 = k_2 = 80$ kN/m represented as blue line and $k_1 = k_2 = 30$ kN/m represented as red line, between 100.0 s and 200.0 s. (For interpretation of the references to colour in this figure legend, the reader is referred to the web version of this article.)

and the maximum displacements of the building structure are 0.05 m, shown in Fig. 19(a). The lateral out of plane displacements of the elevator car relative to the building structure with a high stiffness parameter are almost equal to the displacements of the building structure of 0.05 m, shown in Fig. 19(b), due to the high stiffness parameter representing the stiffness of the tyre-suspension system of the elevator car in the lateral directions. The lateral displacements of the elevator car relative to the building structure with a low stiffness parameter are much higher than the maximum displacements of the building structure as shown in Fig. 20(a) and (b), due to the low stiffness parameter in the lateral directions of the elevator car.

When comparing the lateral in plane displacements of the elevator car relative to the building structure with a high stiffness parameter in Fig. 19(a) with the lateral out of plane displacements of the elevator car with a low stiffness parameter in Fig. 20(b), it is evident that larger displacements of the elevator car are predicted, due to the proximity to the resonance condition, exceeding the allowable limits. However, it should be noted the model limitation is that no damping elements are included in the lateral interface between the guide rails and the elevator car.

In addition the lateral vibrations at the elevator car are induced by irregularities and imperfections of the rail guide system resulting from the accumulation of manufacturing error, which are transmitted to the suspension and compensating ropes resulting in adverse dynamic behaviour of the elevator system, as discussed by Kaczmarczyk and Iwankiewicz [27]. This additional source of excitation induced by irregularities and imperfections of the rail guide system is not taken into account in the model presented in this paper.

3.5. Longitudinal response of the elevator car, compensating sheave and counterweight

The longitudinal displacements of the elevator car, compensating sheave, and counterweight are shown in Figs. 21(a), 22(a), and 23(a) compared when using a high stiffness parameters of $k_1 = k_2 = 80$ kN/m represented as a blue line and a low stiffness parameter of $k_1 = k_2 = 30$ kN/m represented as a red line.

The FFT frequency spectra over a time span of 100.0 s and 150.0 s when using a high stiffness parameters of $k_1 = k_2 = 80$ kN/m represented as a blue line for the elevator car, compensating sheave, and counterweight are shown in Figs. 21(b), 22(b), and 23(b). The predominant frequency is the frequency of 0.84 Hz which is twice the frequency of excitation in the lateral in plane direction coming from the excitation coefficients F_{CR}, F_{CS}, F_{CW} defined in Eqs. (A.35), (A.43), and (A.48) which are the excitation forces acting in the longitudinal direction of the elevator car, compensating sheave, and counterweight, which is primary external excitation.

The primary external excitation in the 1st longitudinal mode which has a predominant frequency of 0.84 Hz, is due to the tuning condition of $\Omega_V \approx \omega_1/2 \approx \omega_1{}^{V/W}$, which in turn provides autoparametric excitation to the first lateral mode leading to 2:1 autoparametric resonance in the system. The elevator car, compensating sheave, and counterweight are in phase as shown in Fig. 7(a) for the vertical mode shapes in the first mode of 0.84 Hz.

The FFT frequency spectra over a time span of 100.0 s and 150.0 s when using a low stiffness parameters of $k_1 = k_2 = 30$ kN/m represented as a red line for the elevator car, compensating sheave, and counterweight are shown in Figs. 21(c), 22(c), and 23(c). The predominant frequency is the frequency of 0.72 Hz which is twice the frequency of excitation in the lateral out of plane direction coming from the excitation co-

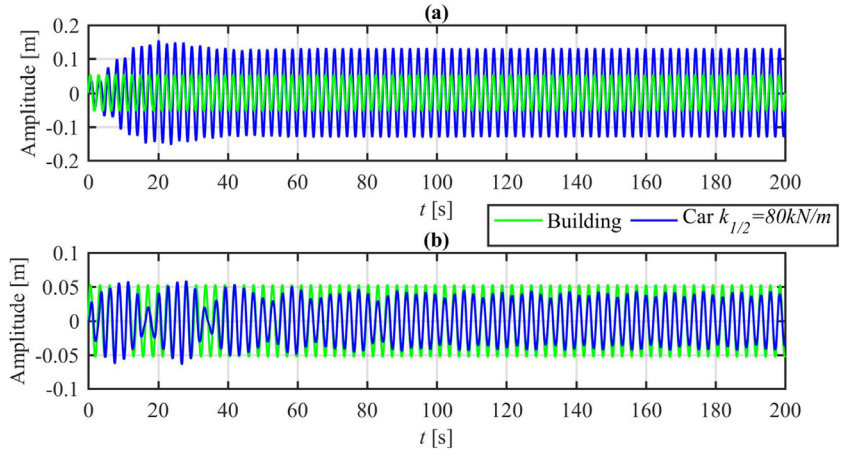

Fig. 19. Lateral displacements of the elevator car relative to the building structure (a) lateral in plane (b) lateral out of plane directions with $k_1 = k_2 = 80$ kN/m represented as a blue line and the displacements of the building structure represented as a green line. (For interpretation of the references to colour in this figure legend, the reader is referred to the web version of this article.)

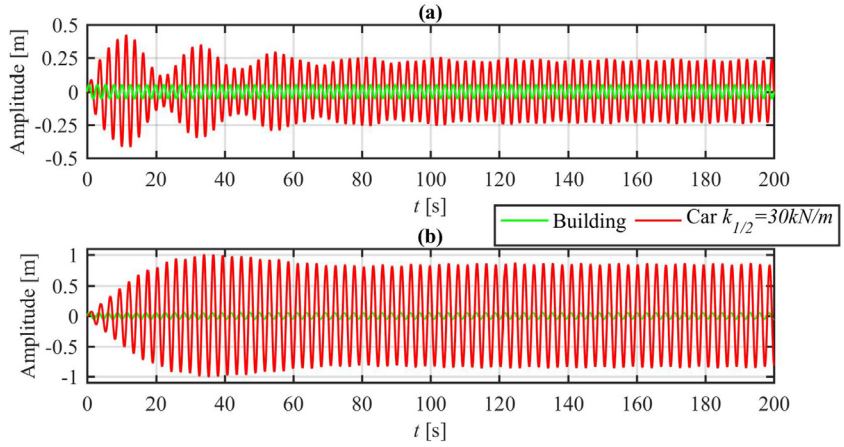

Fig. 20. Lateral displacements of the elevator car relative to the building structure (a) lateral in plane (b) lateral out of plane directions with $k_1 = k_2 = 30$ kN/m represented as a red line and the displacements of the building structure represented as a green line. (For interpretation of the references to colour in this figure legend, the reader is referred to the web version of this article.)

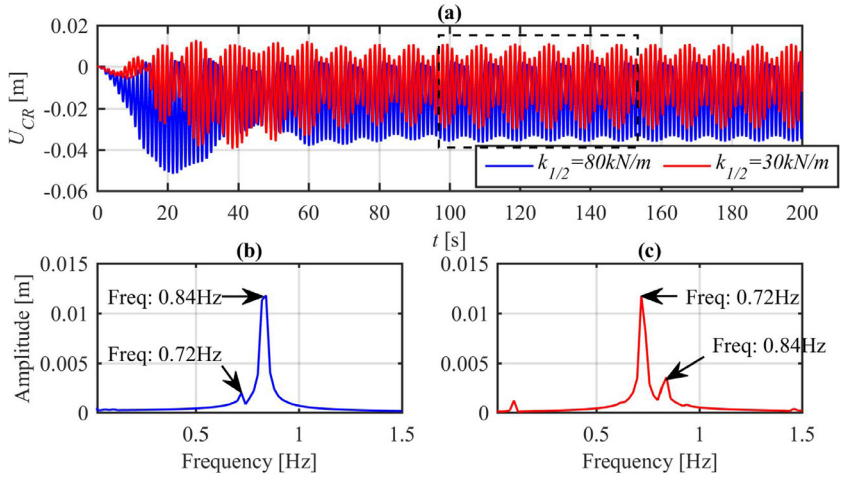

Fig. 21. (a) Longitudinal displacements of the elevator car with $k_1 = k_2 = 80$ kN/m represented as a blue line and $k_1 = k_2 = 30$ kN/m represented as a red line (b, c) FFT frequency spectra of the elevator car between the time span of 100.0 s–150.0 s. (For interpretation of the references to colour in this figure legend, the reader is referred to the web version of this article.)

efficients F_{CR}, F_{CS}, F_{CW} defined in Eqs. (A.35), (A.43), and (A.48) which are the excitation forces acting in the longitudinal direction of the elevator car, compensating sheave, and counterweight, which is primary external excitation.

The mathematical model gives the response of the suspension and compensating ropes at the car and counterweight side and the response of the elevator car in the lateral in plane, lateral out of plane and longitudinal directions with the response in the longitudinal direction of the compensating sheave and counterweight.

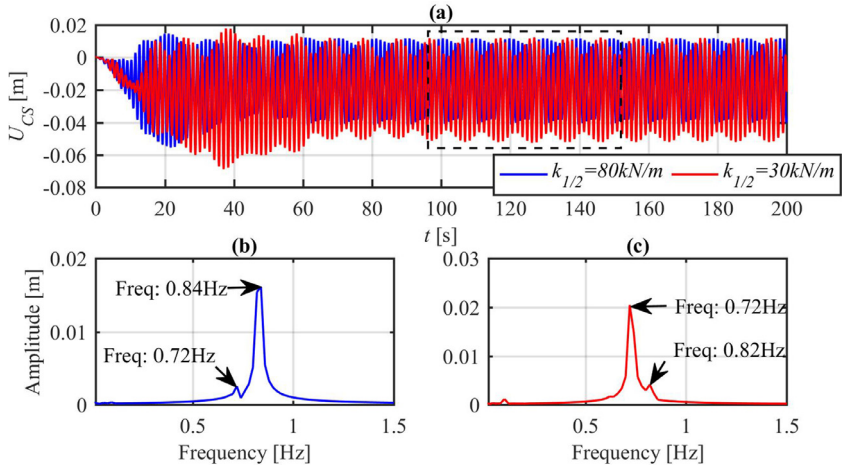

Fig. 22. (a) Longitudinal displacements of the compensating sheave with $k_1 = k_2 = 80$ kN/m represented as a blue line and $k_1 = k_2 = 30$ kN/m represented as a red line (b, c) FFT frequency spectra of the compensating sheave between the time span of 100.0 s–150.0 s. (For interpretation of the references to colour in this figure legend, the reader is referred to the web version of this article.)

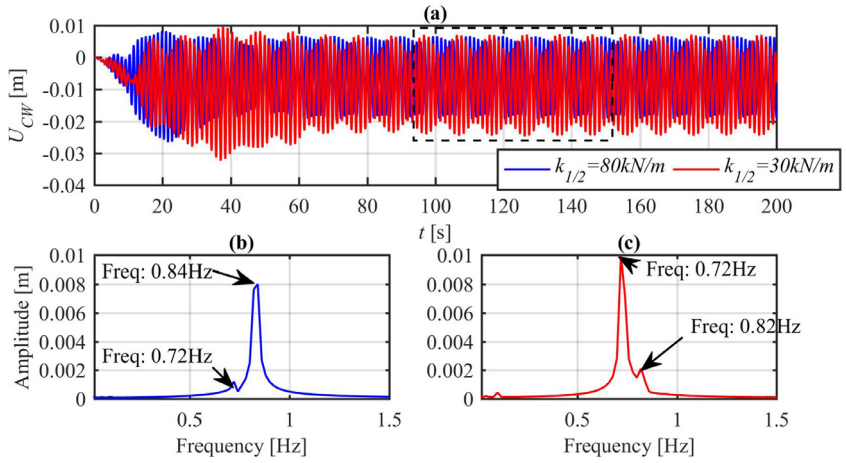

Fig. 23. (a) Longitudinal displacements of the counterweight with $k_1 = k_2 = 80$ kN/m represented as a blue line and $k_1 = k_2 = 30$ kN/m represented as a red line (b, c) FFT frequency spectra of the compensating sheave between the time span of 100.0 s–150.0 s. (For interpretation of the references to colour in this figure legend, the reader is referred to the web version of this article.)

4. Conclusions

The mathematical model of an elevator system derived and presented in this paper takes into account the lateral stiffness of the lift (elevator) car building interface. Green's strain tensor measure for the steel wire rope is applied to express the nonlinear couplings between the modes. The assumption is made that the longitudinal inertia of the ropes can be neglected. This is because in practical applications the longitudinal natural frequencies are much higher than the lateral natural frequencies of the rope and the external excitation frequencies are low. When the elastic interface between the elevator car and the building structure in the lateral directions is considered the veering phenomena appears. The simulation tests are carried out and the results are obtained when the elevator car is positioned at a height where the fundamental natural frequencies of the suspension ropes and compensating ropes at the car side become near each other. It is shown that this particular configuration corresponds to the veering point of the natural frequency loci and is analysed by using high and low stiffness parameters of the lateral stiffness of the car building interface. It is found that the lower the stiffness the more the frequency loci veer away. The lateral response of the suspension ropes, compensating ropes, and the elevator car was high and the ropes would impact the elevator shaft walls and components.

The 1:1 autoparametric internal resonance takes place between the lateral in plane and out of plane modes, due to the effects of the cubic nonlinear terms at the car side. Furthermore, it is shown that the 1st longitudinal mode is excited due to the primary external resonance which in turn acts on the first lateral mode which leads to 2:1 internal resonance. It is demonstrated that the whirling motions of the compensating ropes at the car side take place due to the cubic nonlinear coupling terms between the lateral in plane and out of plane modes. It is evident that large whirling motions occur when the frequency of excitation of the building structure in the lateral in plane and out of plane direction are approximately equal to the fundamental natural frequency of the elevator car, suspension and compensating ropes at the car side.

Due to the ride quality requirements of the elevator system, an elevator car with low lateral stiffness having high lateral vibrations as the ones shown in Figs. 19 and 20 would not be suitable for service. In all cases the resonance responses are too large and some mitigating measures would need to be applied.

Acknowledgements

The financial support received from ThyssenKrupp Elevator AG and the University of Northampton is gratefully acknowledged.

Appendix A

The coefficients $G_{jp}{}^{V1}$ and $G_{jp}{}^{V2}$ are defined in the following equations:

$$G_{jp}^{V1}=\begin{cases} j=p;\ \dfrac{\left(\beta_{1j}^{V}\right)^{2}L_1}{2}+\dfrac{\beta_{1j}^{V}\sin\left(2\beta_{1j}^{V}L_1\right)}{4} \\ j\neq p;\ \beta_{1j}^{V}\beta_{1p}^{V}\left[\dfrac{\sin\left(L_1\left(\beta_{1j}^{V}-\beta_{1p}^{V}\right)\right)}{2\left(\beta_{1j}^{V}-\beta_{1p}^{V}\right)}+\dfrac{\sin\left(L_1\left(\beta_{1j}^{V}+\beta_{1p}^{V}\right)\right)}{2\left(\beta_{1j}^{V}+\beta_{1p}^{V}\right)}\right] \end{cases}, \tag{A.1}$$

$$G_{jp}^{V2}=\begin{cases} j=p;\ \left(\begin{array}{l}\dfrac{L_2\left(\beta_{2j}^{V}\right)^{2}\sin^{2}\beta_{1j}^{V}L_1}{2\sin^{2}\beta_{2j}^{V}L_2}+\dfrac{\beta_{2j}^{V}\sin^{2}\beta_{1j}^{V}L_1\cos 2\beta_{2j}^{V}L_2\sin 2\beta_{2j}^{V}L_2}{4\sin^{2}\beta_{2j}^{V}L_2} \\ +\beta_{2j}^{V}\sin^{2}\beta_{1j}^{V}L_1\cos\beta_{2j}^{V}L_2\sin\beta_{2j}^{V}L_2\end{array}\right) \\ j\neq p;\ \dfrac{1}{\left(\beta_{2p}^{V}\right)^{2}-\left(\beta_{2j}^{V}\right)^{2}}\left(\begin{array}{l}\sin\beta_{2p}^{V}L_2\left(\begin{array}{l}\sin\beta_{2j}^{V}L_2\left(\beta_{2p}^{V}C_{2p}^{V}C_{1j}^{V}-\beta_{2j}^{V}C_{1p}^{V}C_{2j}^{V}\right) \\ +\cos\beta_{2j}^{V}L_2\left(\beta_{2p}^{V}C_{2p}^{V}C_{2j}^{V}+\beta_{2j}^{V}C_{1p}^{V}C_{1j}^{V}\right)\end{array}\right)+ \\ \cos\beta_{2p}^{V}L_2\left(\begin{array}{l}\cos\beta_{2j}^{V}L_2\left(\beta_{2j}^{V}C_{2p}^{V}C_{1j}^{V}-\beta_{2p}^{V}C_{1p}^{V}C_{2j}^{V}\right) \\ -\sin\beta_{2j}^{V}L_2\left(\beta_{2p}^{V}C_{1p}^{V}C_{1j}^{V}+\beta_{2j}^{V}C_{2p}^{V}C_{2j}^{V}\right)\end{array}\right)- \\ \left(\beta_{2j}^{V}C_{2p}^{V}C_{1j}^{V}-\beta_{2p}^{V}C_{1p}^{V}C_{2j}^{V}\right)\end{array}\right) \end{cases}. \tag{A.2}$$

where $C_{1p}^{V}=\beta_{2p}^{V}\sin\beta_{1p}^{V}L_1$, $C_{1j}^{V}=\beta_{2j}^{V}\sin\beta_{1j}^{V}L_1$, $C_{2j}^{V}=\frac{\beta_{2j}^{V}\sin\beta_{1j}^{V}L_1\cos\beta_{2j}^{V}L_2}{\sin\beta_{2j}^{V}L_2}$, and $C_{2p}^{V}=\frac{\beta_{2p}^{V}\sin\beta_{1p}^{V}L_1\cos\beta_{2p}^{V}L_2}{\sin\beta_{2p}^{V}L_2}$.

Similarly, $G_{jp}{}^{W1}$ and $G_{jp}{}^{W2}$ can be deducted. The coefficients for the subsystem at the car side composed of the elevator car, suspension, and compensating ropes in the lateral in plane direction defined in Eq. (88) are presented in the following equations:.

$$m_{rr}^{V}=m_1\int_0^{L_1}\phi_{1r}^{2}(x_1)dx_1+M_1\phi_{1r}^{2}(L_1)+m_2\int_0^{L_2}\phi_{2r}^{2}(x_2)dx_2, \tag{A.3}$$

$$\left(\omega_{rr}^{V}\right)^{2}=\begin{bmatrix}-\left(M_1+m_1L_1+m_2L_2+\frac{M_2}{2}\right)g\int_0^{L_1}\phi''_{1r}(x_1)\phi_{1r}(x_1)dx_1 \\ +\left(M_1+m_2L_2+\frac{M_2}{2}\right)g\phi'_{1r}(L_1)\phi_{1r}(L_1) \\ +2k_1\phi_{1r}(L_1)^{2}-\left(m_2L_2+\frac{M_2}{2}\right)g\int_0^{L_2}\phi''_{2r}(x_2)\phi_{2r}(x_2)dx_2 \\ -\left(m_2L_2+\frac{M_2}{2}\right)g\phi'_{2r}(0)\phi_{1r}(L_1)\end{bmatrix}/m_{rr}^{V}, \tag{A.4}$$

$$k_{rn}^{V1}=\begin{bmatrix}m_1g\left(\int_0^{L_1}x_1\phi''_{1n}(x_1)\phi_{1r}(x_1)dx_1+\int_0^{L_1}\phi'_{1n}(x_1)\phi_{1r}(x_1)dx_1\right) \\ +\frac{EA_1\left(\left(\xi_1^{V}-S_V\right)^{2}+\left(\xi_1^{W}-S_W\right)^{2}\right)}{2L_1^{2}}\left(-\int_0^{L_1}\phi''_{1n}(x_1)\phi_{1r}(x_1)dx_1+\phi'_{1n}(L_1)\phi_{1r}(L_1)\right) \\ +\left(\frac{EA_1\left(\xi_1^{V}-S_V\right)^{2}}{L_1^{3}}+\frac{EA_2\left(\xi_1^{V}\right)^{2}}{L_2^{3}}\right)\phi_{1n}(L_1)\phi_{1r}(L_1) \\ -\frac{EA_2\left(\left(\xi_1^{V}\right)^{2}+\left(\xi_1^{W}\right)^{2}\right)}{2L_2^{2}}\left(\int_0^{L_2}\phi''_{2n}(x_2)\phi_{2r}(x_2)dx_2+\phi'_{2n}(0)\phi_{1r}(L_1)\right) \\ +m_2g\left(\int_0^{L_2}x_2\phi''_{2n}(x_2)\phi_{2r}(x_2)dx_2+\int_0^{L_2}\phi'_{2n}(x_2)\phi_{2r}(x_2)dx_2\right)\end{bmatrix}/m_{rr}^{V}, \tag{A.5}$$

$$k_{rn}^{V2}=\frac{\alpha_{1n}(L_1)\phi_{1r}(L_1)}{m_{rr}^{V}}\left(\frac{EA_1\left(\xi_1^{V}-S_V\right)\left(\xi_1^{W}-S_W\right)}{L_1^{3}}+\frac{EA_2\xi_1^{V}\xi_1^{W}}{L_2^{3}}\right), \tag{A.6}$$

$$k_{r}^{V3}=\frac{\phi_{1r}(L_1)}{m_{rr}^{V}}\left(\frac{EA_1\left(\xi_1^{V}-S_V\right)}{L_1^{2}}-\frac{EA_2\xi_1^{V}}{L_2^{2}}\right), \tag{A.7}$$

$$k_{r}^{V4}=\frac{EA_2\xi_1^{V}\phi_{1r}(L_1)}{m_{rr}^{V}L_2^{2}}, \tag{A.8}$$

$$D_{rn}^{V1}=\frac{EA_1\left(\xi_1^{V}-S_V\right)\phi_{1r}(L_1)}{m_{rr}^{V}L_1^{2}}\left(-\int_0^{L_1}\phi''_{1n}(x_1)\phi_{1r}(x_1)dx_1+\phi_{1j}(L_1)\phi'_{1n}(L_1)+\frac{G_{jp}^{V1}}{2}\right)+\frac{EA_2\xi_1^{V}\phi_{1r}(L_1)}{m_{rr}^{V}L_2^{2}}\left(-\int_0^{L_2}\phi''_{2n}(x_2)\phi_{2r}(x_2)dx_2-\phi_{1j}(L_1)\phi'_{2n}(0)+\frac{G_{jp}^{V2}}{2}\right), \tag{A.9}$$

$$D_{rn}^{V2}=\frac{EA_1\left(\xi_1^{W}-S_W\right)\alpha_{1j}(L_1)}{m_{rr}^{W}L_1^{2}}\left(-\int_0^{L_1}\phi''_{1n}(x_1)\phi_{1r}(x_1)dx_1+\phi_{1r}(L_1)\phi'_{1n}(L_1)\right)+\frac{EA_2\xi_1^{W}\alpha_{1j}(L_1)}{m_{rr}^{V}L_2^{2}}\left(-\int_0^{L_2}\phi''_{2n}(x_2)\phi_{2r}(x_2)dx_2-\phi_{1r}(L_1)\phi'_{2n}(0)\right), \tag{A.10}$$

$$D_{rn}^{V3}=\frac{\phi_{1r}(L_1)}{2m_{rr}^{V}}\left(\frac{EA_1\left(\xi_1^{V}-S_V\right)}{L_1^{2}}G_{jp}^{W1}+\frac{EA_2\xi_1^{V}}{L_2^{2}}G_{jp}^{W2}\right), \tag{A.11}$$

$$D_{rn}^{V4}=-\frac{EA_1}{L_1m_{rr}^{V}}\left(\int_0^{L_1}\phi''_{1n}(x_1)\phi_{1r}(x_1)dx_1-\phi'_{1n}(L_1)\phi_{1r}(L_1)\right)+\frac{EA_2}{L_2m_{rr}^{V}}\left(\int_0^{L_2}\phi''_{2n}(x_2)\phi_{2r}(x_2)dx_2-\phi'_{2n}(0)\phi_{1r}(L_1)\right), \tag{A.12}$$

$$D_{rn}^{V5}=-\frac{EA_2}{L_2m_{rr}^{V}}\left(\int_0^{L_2}\phi''_{2n}(x_2)\phi_{2r}(x_2)dx_2-\phi'_{2n}(0)\phi_{1r}(L_1)\right), \tag{A.13}$$

$$R_{rnjp}^{V1}=R_{rnjp}^{V2}=\frac{EA_1G_{jp}^{V1/W1}}{2m_{rr}^{V}L_1}\left(-\int_0^{L_1}\phi''_{1n}(x_1)\phi_{1r}(x_1)dx_1+\phi'_{1n}(L_1)\phi_{1r}(L_1)\right)-\frac{EA_2G_{jp}^{V2/W2}}{2m_{rr}^{V}L_2}\left(\int_0^{L_2}\phi''_{2n}(x_2)\phi_{2r}(x_2)dx_2+\phi'_{2n}(0)\phi_{1r}(L_1)\right), \tag{A.14}$$

$$F_r^{V}=\frac{m_1}{m_{rr}^{V}L_1}\begin{pmatrix}\left(-\lambda_V^{2}L_1S_V+\xi_1^{V}g-S_Vg\right)\int_0^{L_1}\phi_{1r}(x_1)dx_1 \\ -\left(\xi_1^{V}-S_V\right)\lambda_V^{2}\int_0^{L_1}x_1\phi_{1r}(x_1)dx_1\end{pmatrix}+\begin{pmatrix}\left(M_1+m_2L_2+\frac{M_2}{2}\right)\frac{g\left(\xi_1^{V}-S_V\right)}{L_1}+\left(\frac{M_2}{2}+m_2L_2\right)\frac{g\xi_1^{V}}{L_2} \\ -M_1\xi_1^{V}\lambda_V^{2}+\frac{EA_1\left(\xi_1^{V}-S_V\right)}{2L_1^{3}}\left(\left(\xi_1^{V}-S_V\right)^{2}+\left(\xi_1^{W}-S_W\right)^{2}\right) \\ +\frac{EA_2\xi_1^{V}}{2L_2^{3}}\left(\left(\xi_1^{V}\right)^{2}+\left(\xi_1^{W}\right)^{2}\right)\end{pmatrix}\frac{\phi_{1r}(L_1)}{m_{rr}^{V}}\cdot+\frac{m_2\xi_1^{V}}{m_{rr}^{V}L_2}\left(-\left(L_2\lambda_v^{2}+g\right)\int_0^{L_2}\phi_{2r}(x_2)dx_2+\lambda_V^{2}\int_0^{L_2}x_2\phi_{2r}(x_2)dx_2\right) \tag{A.15}$$

The coefficients for the subsystem at the car side composed of the elevator car, suspension and compensating ropes in the lateral out of plane direction defined in Eq. (89) can be derived by following the same procedure. The coefficients of Eq. (90) representing the compensating rope at the counterweight side ($i=3$) in the lateral in plane direction are presented in the following equations:

$$m_{3rr}^{V}=m_2\int_0^{L_3}\phi_{3r}^{2}(x_3)dx_3, \tag{A.16}$$

$$\left(\omega_{3rr}^{V}\right)^{2}=-\left(m_2L_3+\frac{M_2}{2}\right)\frac{g}{m_{3rr}^{V}}\int_0^{L_3}\phi''_{3r}(x_3)\phi_{3r}(x_3)dx_3+\frac{m_2g}{m_{3rr}^{V}}\left(\int_0^{L_3}\phi'_{3r}(x_3)\phi_{3r}(x_3)dx_3+\int_0^{L_3}x_3\phi''_{3r}(x_3)\phi_{3r}(x_3)dx_3\right), \tag{A.17}$$

$$k_{3rn}^{V} = -\frac{EA_2\left(\left(\xi_2^V\right)^2 + \left(\xi_2^W\right)^2\right)}{2L_3^2 m_{3rr}^V}\int_0^{L_3} \phi''_{3n}(x_3)\phi_{3r}(x_3)dx_3, \tag{A.18}$$

$$D_{3rn}^{V1} = -\frac{EA_2}{L_3 m_{3rr}^V}\int_0^{L_3} \phi''_{3n}(x_3)\phi_{3r}(x_3)dx_3, \tag{A.19}$$

$$D_{3rn}^{V2} = \frac{EA_2}{L_3 m_{3rr}^V}\int_0^{L_3} \phi''_{3n}(x_3)\phi_{3r}(x_3)dx_3, \tag{A.20}$$

$$R_{3rnjp}^{V1} = R_{3rnjp}^{V2} = -\frac{EA_2}{4m_{3rr}^V}\left(\frac{jp\pi}{L_3}\right)^2\int_0^{L_3} \phi''_{3n}(x_3)\phi_{3r}(x_3)dx_3, \tag{A.21}$$

$$F_{3r}^{V} = \frac{m_2\xi_2^V}{m_{3rr}^V L_3}\left(-\left(L_3\lambda_V^2 + g\right)\int_0^{L_3}\phi_{3r}(x_3)dx_3 + \lambda_V^2\int_0^{L_3} x_3\phi_{3r}(x_3)dx_3\right). \tag{A.22}$$

The coefficients of Eq. (90) representing the suspension rope at the counterweight side ($i=4$) in the lateral in plane direction are presented in the following equations:

$$m_{4rr}^V = m_1\int_0^{L_4}\phi_{4r}^2(x_4)dx_4, \tag{A.23}$$

$$\begin{aligned}\left(\omega_{4rr}^V\right)^2 = &-\left(M_3 + m_1L_4 + m_2L_3 + \tfrac{M_2}{2}\right)\tfrac{g}{m_{4rr}^V}\textstyle\int_0^{L_4}\phi''_{4r}(x_4)\phi_{4r}(x_4)dx_4\\ &+\tfrac{m_1 g}{m_{4rr}^V}\left(\textstyle\int_0^{L_4} x_4\phi''_{4n}(x_4)\phi_{4r}(x_4)dx_4 + \int_0^{L_4}\phi'_{4n}(x_4)\phi_{4r}(x_4)dx_4\right)\end{aligned}, \tag{A.24}$$

$$k_{4rn}^{V} = -\frac{EA_1\left(\left(\xi_2^V - \xi_3^V\right)^2 + \left(\xi_2^W - \xi_3^W\right)^2\right)}{2m_{4rr}^V L_4^2}\int_0^{L_4}\phi''_{4n}(x_4)\phi_{4r}(x_4)dx_4, \tag{A.25}$$

$$D_{4rn}^{V1} = 0, \tag{A.26}$$

$$D_{4rn}^{V2} = -\frac{EA_1}{m_{4rr}^V L_4}\int_0^{L_4}\phi''_{4n}(x_4)\phi_{4r}(x_4)dx_4, \tag{A.27}$$

$$R_{4rnjp}^{V1} = R_{4rnjp}^{V2} = -\frac{EA_1}{4m_{4rr}^V}\left(\frac{jp\pi}{L_4}\right)^2\int_0^{L_4}\phi''_{4n}(x_4)\phi_{4r}(x_4)dx_4, \tag{A.28}$$

$$\begin{aligned}F_{4r}^{V} = &\frac{m_1}{m_{4rr}^V L_4}\left(-\xi_3^V L_4\lambda_V^2 + g\xi_2^V - g\xi_3^V\right)\int_0^{L_4}\phi_{4r}(x_4)dx_4\\ &-\frac{m_1\lambda_V^2\left(\xi_2^V - \xi_3^V\right)}{m_{4rr}^V L_4}\int_0^{L_4} x_4\phi_{4r}(x_4)dx_4.\end{aligned} \tag{A.29}$$

The coefficients of Eq. (91) representing the compensating rope ($i=3$) and the suspension rope ($i=4$) at the counterweight side in the lateral out of plane direction can be deducted. The coefficients of Eq. (73) representing the dynamic response of the elevator car in the longitudinal direction are presented in the following equations:

$$k^{u1} = \frac{EA_1}{L_1} + \frac{EA_2}{L_2}, \tag{A.30}$$

$$k^{u2} = -\frac{EA_2}{L_2}, \tag{A.31}$$

$$k_n^{u3} = \left(\frac{EA_1\left(\xi_1^V - S_V\right)}{L_1^2} - \frac{EA_2\xi_1^V}{L_2^2}\right)\phi_{1n}(L_1), \tag{A.32}$$

$$k_n^{u4} = \left(\frac{EA_1\left(\xi_1^W - S_W\right)}{L_1^2} - \frac{EA_2\xi_1^W}{L_2^2}\right)\alpha_{1n}(L_1), \tag{A.33}$$

$$R_{jp}^{u1} = R_{jp}^{u2} = \frac{EA_1}{2L_1}G_{jp}^{V1/W1} - \frac{EA_2}{2L_2}G_{jp}^{V2/W2}, \tag{A.34}$$

$$f_{CR} = \frac{EA_1}{2L_1^2}\left(\left(\xi_1^V - S_V\right)^2 + \left(\xi_1^W - S_W\right)^2\right) - \frac{EA_2}{2L_2^2}\left(\left(\xi_1^V\right)^2 + \left(\xi_1^W\right)^2\right). \tag{A.35}$$

The coefficients of Eq. (74) representing the dynamic responses of the compensating sheave in the longitudinal direction are presented in the following equations:

$$\bar{k}^{u1} = -\frac{EA_2}{L_2}, \tag{A.36}$$

$$\bar{k}^{u2} = EA_2\left(\frac{1}{L_2} + \frac{1}{L_3}\right), \tag{A.37}$$

$$\bar{k}^{u3} = -\frac{EA_2}{L_3}, \tag{A.38}$$

$$\bar{k}_n^{u4} = -\frac{EA_2\xi_1^V}{L_2^2}\phi_{2n}(L_2), \tag{A.39}$$

$$\bar{k}_n^{u5} = -\frac{EA_2\xi_1^W}{L_2^2}\alpha_{2n}(L_2), \tag{A.40}$$

$$\bar{R}_{jp}^{u1} = \bar{R}_{jp}^{u2} = -\frac{EA_2}{2L_2}G_{jp}^{V2/W2}, \tag{A.41}$$

$$\bar{R}_n^{u3} = \bar{R}_n^{u4} = \frac{EA_2}{4}\left(\frac{n\pi}{L_3}\right)^2, \tag{A.42}$$

$$f_{CS} = \frac{EA_2}{2}\left(\left(\frac{\xi_1^V}{L_2}\right)^2 + \left(\frac{\xi_1^W}{L_2}\right)^2 + \left(\frac{\xi_2^V}{L_3}\right)^2 + \left(\frac{\xi_1^W}{L_3}\right)^2\right). \tag{A.43}$$

The coefficients of Eq. (75) representing the dynamic responses of the counterweight in the longitudinal direction are presented in the following equations:

$$\hat{k}^{u1} = -\frac{EA_2}{L_3}, \tag{A.44}$$

$$\hat{k}^{u2} = \frac{EA_2}{L_3} + \frac{EA_1}{L_4}, \tag{A.45}$$

$$\hat{R}_n^{u1} = \hat{R}_n^{u2} = -\frac{EA_2}{4}\left(\frac{n\pi}{L_3}\right)^2, \tag{A.46}$$

$$\hat{R}_n^{u3} = \hat{R}_n^{u4} = \frac{EA_1}{4}\left(\frac{n\pi}{L_4}\right)^2, \tag{A.47}$$

$$f_{CW} = \frac{EA_1}{2}\left(\left(\frac{\xi_2^V - \xi_3^V}{L_4}\right)^2 + \left(\frac{\xi_2^W - \xi_3^W}{L_4}\right)^2\right) - \frac{EA_2}{2}\left(\left(\frac{\xi_2^V}{L_3}\right)^2 + \left(\frac{\xi_2^W}{L_3}\right)^2\right). \tag{A.48}$$

References

[1] Clemente P, Marulo F, Lecce L, Bifulco A. Experimental modal analysis of the Garigliano cable-stayed bridge. Soil Dyn Earthq Eng 1998;17:485–93. doi:10.1016/S0267-7261(98)00022-0.

[2] Huang K, Feng Q, Yin Y. Nonlinear vibration of the coupled structure of suspended-cable-stayed beam – 1:2 internal resonance. Acta Mech Solida Sin 2014;27:467–76. doi:10.1016/S0894-9166(14)60055-0.

[3] Desai YM, Punde S. Simple model for dynamic analysis of cable supported structures. Eng Struct 2000;23:271–9. doi:10.1016/S0141-0296(00)00035-3.

[4] Cha J-H, Roh M-I, Lee K-Y. Dynamic response simulation of a heavy cargo suspended by a floating crane based on multibody system dynamics. Ocean Eng 2010;37:1273–91. doi:10.1016/j.oceaneng.2010.06.008.

[5] Kevac L, Filipovic M, Rakic A. Dynamics of the process of the rope winding (unwinding) on the winch. Appl Math Model 2017;48:821–43. doi:10.1016/j.apm.2017.02.023.

[6] Kaczmarczyk S, Picton P. The prediction of nonlinear responses and active stiffness control of moving slender continua subjected to dynamic loadings in a vertical host structure. Int J Acoust Vib 2012;18:39–44.

[7] Kaczmarczyk S. The passage through resonance in a catenary-vertical cable hoisting system with slowly varying length. J Sound Vib 1997;208:243–69.

[8] Kaczmarczyk S, Ostachowicz W. Transient vibration phenomena in deep mine hoisting cables. Part 1: mathematical model. J Sound Vib 2003;262:219–44. doi:10.1016/S0022-460X(02)01137-9.

[9] Kaczmarczyk S, Ostachowicz W. Transient vibration phenomena in deep mine hoisting cables. Part 2: numerical simulation of the dynamics response. J Sound Vib 2003;262:219–44. doi:10.1016/S0022-460X(02)01137-9.

[10] Kaczmarczyk S, Mirhadizadeh S, Picton P, Salamaliki-Simpson R, Turner S. Modelling, simulation and experimental validation of nonlinear dynamic interactions in an aramid rope system. In: Proceedings of the eleventh international conference of vibration problems, Lisbon; 2013.

[11] Zhu WD, Ren H. An accurate spatial discretization and substructure method with application to moving elevator cable-car systems—Part I: application. J Vib Acoust 2013;135:051036, 10 pages. doi:10.1115/1.4024558.

[12] Ren H, Zhu WD. An accurate spatial discretization and substructure method with application to moving elevator cable-car systems—Part II: application. J Vib Acoust 2013;135. doi:10.1115/1.4024558.

[13] Thomsen JJ. Theories and experiments on the stiffening effect of high-frequency excitation for continuous elastic systems. J Sound Vib 2003;260:117–39. doi:10.1016/S0022-460X(02)00916-1.

[14] Sandilo SH, van Horssen WT. On variable length induced vibrations of a vertical string. J Sound Vib 2014;333:2432–49. doi:10.1016/j.jsv.2014.01.011.

[15] Zhu WD, Xu GY. Vibration of elevator cables with small bending stiffness. J Sound Vib 2003;263:679–99. doi:10.1016/S0022-460X(02)01468-2.

[16] Watanabe S, Okawa T, Nakazawa D. Vertical vibration analysis for elevator compensating sheave. In: Proceedings of the eleventh international conference of vibration problems, Lisbon; 2013.

[17] Chi RM, Shu HT. Longitudinal vibration of a hoist rope coupled with the vertical vibration of an elevator car. J Sound Vib 1991;148:154–9.

[18] Arrasate X, Kaczmarczyk S, Almandoz G, Abete JM, Isasa I. Measurement and simulation of machine-borne vertical vibration in elevator systems. In: Proceedings of the eleventh international conference of vibration problems, Lisbon; 2013.

[19] Nakazawa D, Watanabe S, Fukui D, Okawa T. Lateral vibration analysis for elevator compensation rope. In: Proceedings of the eleventh international conference of vibration problems, Lisbon; 2013.

[20] Kimura H, Kuguminato T. Simplified calculation method for detecting elevator rope deflection during earthquake (considering the distribution of rope tension). Trans Jpn Soc Mech Eng Ser C 2013;79:1237–46. doi:10.1299/kikaic.79.1237.

[21] Wang Z, Hong M, Xu J, Cui H. Analytical and experimental study of free vibration of beams carrying multiple masses and springs. J Mar Sci Appl 2014;13:32–40. doi:10.1007/s11804-014-1231-4.

[22] Öztürk H, Sabuncu M. Stability analysis of a cantilever composite beam on elastic supports. Compos Sci Technol 2005;65:1982–95. doi:10.1016/j.compscitech.2005.03.004.

[23] Riedel CH, Tan CA. Coupled, forced response of an axially moving strip with internal resonance. Int J Non-Linear Mech 2002;37:101–16. doi:10.1016/S0020-7462(00)00100-1.

[24] Park S, Chung J. Dynamic analysis of an axially moving finite-length beam with intermediate spring supports. J Sound Vib 2014;333:6742–59. doi:10.1016/j.jsv.2014.07.031.

[25] Kimura H. Forced vibration analysis of an axially moving string with constant length. J Syst Des Dyn 2011;5:1546–58. doi:10.1299/jsdd.5.1546.

[26] Moon J, Wickert JA. Non-linear vibration of power transmission belts. J Sound Vib 1997;200:419–31. doi:10.1006/jsvi.1996.0709.

[27] Kaczmarczyk S, Iwankiewicz R. Dynamic response of an elevator car due to stochastic rail excitation. Proceeding of the 2006 Estonian academy of sciences, physics and mathematics Estonia; 2006.

[28] Strakosch GR. The vertical transportation handbook. New York: Jon Wiley and Sons; 1998.

[29] Lopez SMR, Perondi EA, Sobrinho MRS. Adaptive control for an active suspension of an elevator. ABCM Symp Ser Mechatron 2010;4:62–71.

[30] Yamazaki Y, Tmomisawa M, Okada K, Sugiyama Y. Vibration control of super-high-speed elevators. Proceeding of the fourteenth international modal analysis conference Dearborn, USA; 1996.

[31] Kaczmarczyk S, Iwankiewicz R. Nonlinear vibrations of a cable system with a tuned mass damper under deterministic and stochastic base excitation. Proc Eng 2017;199:675–80. doi:10.1016/j.proeng.2017.09.587.

[32] Yang DH, Kim KY, Kwak MK, Lee S. Dynamic modeling and experiments on the coupled vibrations of building and elevator ropes. J Sound Vib 2017;390:164–91. doi:10.1016/j.jsv.2016.10.045.

[33] Al-Kodmany K. Tall buildings and elevators: a review of recent technological advances. Buildings 2015;5:1070–104. doi:10.3390/buildings5031070.

[34] Meirovitch L. Fundamentals of vibrations. Singapore: McGraw-Hill Book Co; 2001.

[35] Andrew J, Kaczmarczyk S. Systems engineering of elevators. Mobile, Alabama, USA: Elevator World, Inc.; 2011.

[36] British Standards Institute. Safety rules for the construction and installation of lifts – examinations and tests Part 50: design rules, calculations, examinations and tests of lifts components, London: BSI; 2014. BS EN 81-50:2014.

[37] Salamaliki-Simpson R. The modelling and simulation of the dynamic behaviour of a lift car-rope suspension system Ph.D. thesis. The University of Northampton; 2009.

[38] Nayfeh AH, Mook DT. Nonlinear oscillations. USA: Jon Wiley and Sons; 1979.

[39] Michael R, Roth D, Ruskey R, Ferro E. The study of a neoprene elevator roller guide. In: Proceedings of the ANSYS user's conference, Pennsylvania, USA; 2004 consumer products session.

[40] Kijewski-Correa T, Kochly M. Monitoring the wind-induced response of tall buildings: GPS performance and the issue of multipath effects. J Wind Eng Ind Aerodyn 2007;95:1176–98. doi:10.1016/j.jweia.2007.02.002.

[41] Mendis P, Ngo T, Haritos N, Hira A, Samali B, Cheung J. Wind loading on tall buildings. EJSE Spec Issue Load Struct 2007;3:41–54.

[42] Bashor R, Bobby S, Kijewski-Correa T, Kareem A. Full-scale performance evaluation of tall buildings under wind. J Wind Eng Ind Aerodyn 2012;104–106:88–97. doi:10.1016/j.jweia.2012.04.007.

[43] Kijewski-Correa T, Pirnia JD. Dynamic behavior of tall buildings under wind: insights from full-scale monitoring. Struct Des Tall Spec Build 2007;16:471–86. doi:10.1002/tal.415.

[44] Kijewski-correa T, Kilpatrick J, Kwon D, Bashor R, Bradley S, Abdelrazaq A, et al. Full-scale validation of the wind-induced response of tall buildings: updated findings from the Chicago monitoring project. In: Proceedings of the tenth Americas conference on wind engineering; 2005.

[45] Giannini O, Sestieri A. Experimental characterization of veering crossing and lock-in in simple mechanical systems. Mech Syst Signal Process 2016;72–73:846–64. doi:10.1016/j.ymssp.2015.11.012.

[46] du Bois JL, Adhikari S, Lieven NJ. On the quantification of eigenvalue curve veering: a veering index. J Appl Mech 2011;78:041007, 8 pages. doi:10.1115/1.4003189.

[47] Bendiksen OO. Localization phenomena in structural dynamics. Chaos Solitons Fractals 2000;11:1621–60. doi:10.1016/S0960-0779(00)00013-8.

[48] Pierre C, Plaut RH. Curve veering and mode localization in a buckling problem. J Appl Math Phys 1989;40:758–61. doi:10.1007/BF00945875.